

1 **Shoreline and Land Use Land Cover Changes along the 2004 tsunami-**
2 **affected South Andaman Coast: Understanding Changing Hazard**
3 **Susceptibility**

4 Vikas Ghadamode^{1,2}, Aruna Kumari Kondarathi¹, Anand K Pandey^{1,2,§} Kirti Srivastava¹

5 1. CSIR- National Geophysical Research Institute, Hyderabad, 500007 India.

6 2. Academy of Scientific and Innovative Research (AcSIR), Ghaziabad 201002, India.

7

8 § Corresponding author: Email address: akpandey@ngri.res.in

9 *Tel: +91-40-27012416*

10

11

12 **Abstract**

13 The 2004 tsunami affected the South Andaman coast, experiencing dynamic changes in the
14 coastal geomorphology, making the region vulnerable. We focus on pre-and post-tsunami
15 shoreline and Land Use Land Cover changes for 2004, 2005, and 2022 to analyse the dynamic
16 change in hazard. We used GEBCO bathymetry data to calculate Run-up (m), arrival times
17 (Min), and inundation (m) at a few locations using three tsunamigenic earthquake source
18 parameters, namely the 2004-Sumatra, 1941-North Andaman, and 1881-Car Nicobar
19 earthquakes. The Digital Shoreline Analysis System is used for the shoreline change estimates.
20 The Landsat data is used to calculate shoreline and Land Use Land Cover (LULC) change in
21 five classes, namely Built-Up Areas, Forests, Inundation areas, Croplands, and water bodies
22 during the above period. We examine the correlation between the LULC changes and the
23 dynamic change in shoreline due to population flux, infrastructural growth, and Gross State
24 Domestic Product growth. India industry estimates the Andaman & Nicobar Islands losses
25 exceed INR 10 billion during 2004, which would see a five-fold increase in economic loss due
26 to a doubling of built-up area, a three-fold increase in tourist inflow, and a population density
27 growth. The unsustainable decline in the forest cover, mangroves, and cropland would affect
28 sustainability during a disaster despite coastal safety measures.

29 **Keywords: Geomorphology, Land use Land cover, Shoreline, Tsunami, Remote sensing**

30

31 **1. Introduction:**

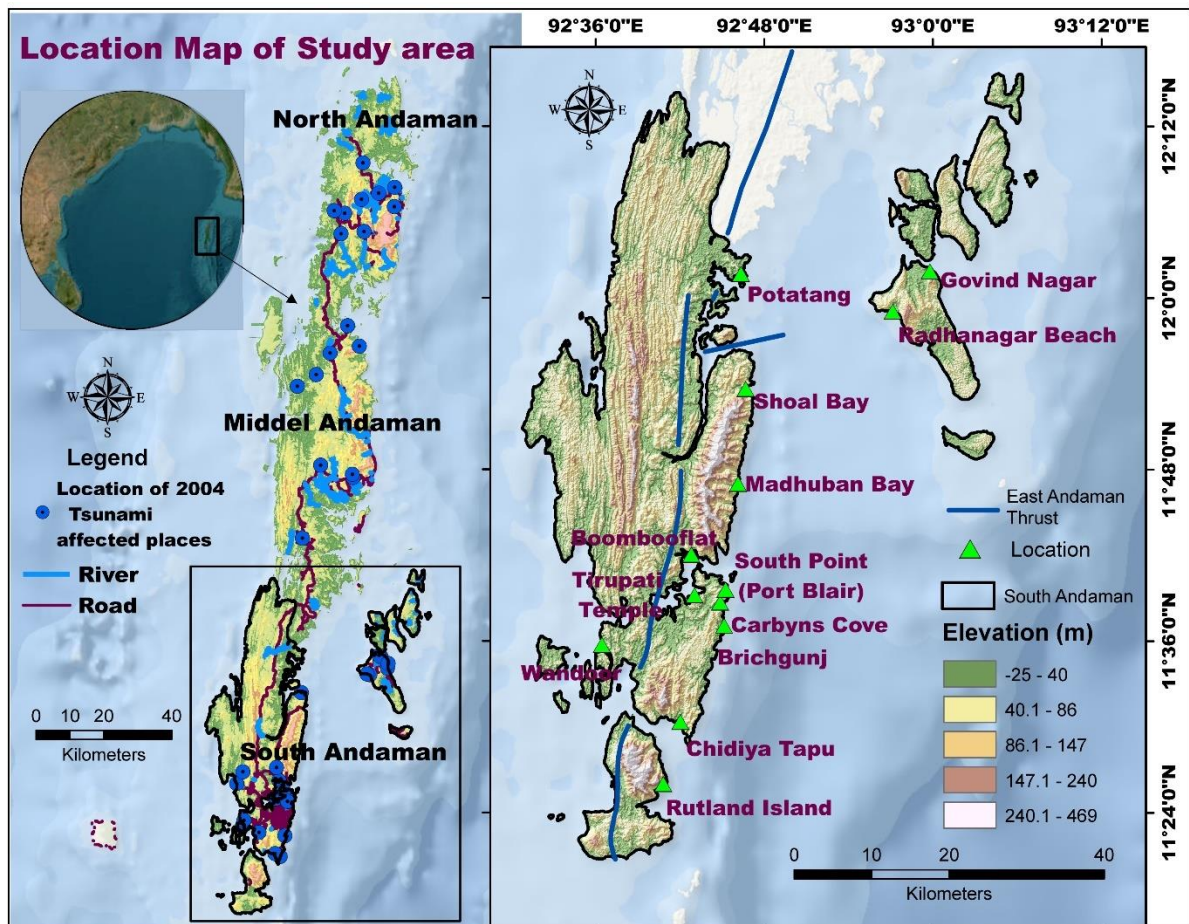
32 The Coastal shorelines are dynamic and highly vulnerable to erosion and accretion caused
33 by hydrodynamic, tectonic, geomorphic, and climate forcing, including tsunamis, cyclones,
34 flooding, storm surges, wave action, wind and tide changes, and sea level variations (Nayak
35 2002; Boak & Turner 2005; Kumar et al., 2010; Mukhopadhyay et al., 2011). In addition to
36 natural coastal processes, coastal resources are constantly under stress due to anthropogenic
37 activities, such as industrialization, port construction, beach sand mining, garbage dumping,
38 urbanization, trade, tourism, and recreational activities, which significantly impact the
39 shoreline and results into damage to natural ecosystems (Yi et al., 2018; Davis, 2019). It is
40 important to regularly monitor spatiotemporal along shorelines, Land use / Land Cover
41 (LULC), and geomorphic features (Moran, 2003; Cooper et al., 2004; Scheffers et al., 2005;
42 Jayakumar & Malarvannan, 2016). Several studies have analyzed various coastal processes,
43 including mapping shoreline change, LULC change detection, and analysis of
44 geomorphological landforms using satellite data. The temporal multispectral satellite data
45 allow for the identification of regions undergoing erosion or accretion change (Misra and
46 Balaji, 2015; Kumari et al., 2012; Tonisso et al., 2012; Murali et al., 2013; Sudha Rani et al.,
47 2015; Rowland et al., 2022; Thiéblemont et al., 2021). The M 9.3 undersea earthquake on
48 December 26, 2004, near the coast of Sumatra, Indonesia, triggered the Indian Ocean tsunami
49 and caused massive destruction of the coastal ecosystem in the Andaman region (Sheth et al.,
50 2006; Ramalanjaona, 2011). Several researchers analyzed shoreline and geomorphological
51 changes of the 2004 Sumatra tsunami using remote sensing data (Kumari et al., 2012; Yuvaraj
52 et al., 2014; Yunus and Narayana, 2015; Yunus et al., 2016).

53 Since the 2004 tsunami, the Andaman and Nicobar Islands have experienced notable
54 population growth, infrastructural development, and flourishing tourism activities over the past
55 decade (Yuvaraj et al., 2014). The development is profound in the south Andaman region. This

56 is a cause of concern for the tsunami vulnerability as the region is prone to large earthquakes
57 and is a seismo-tectonically active plate boundary. In this study, we Compute Tsunami arrival
58 times, run-up heights, and inundation extent along the south Andaman region. We also
59 analyzed dynamic vulnerability using temporal and spatial changes in shoreline and LULC for
60 the tsunami-affected areas (Velmurugan et al., 2006; Ghadamode et al., 2022). The analysis
61 covers three time periods: 2004 (pre-tsunami), 2005 (post-tsunami), and 2022 (current state) of
62 shoreline changes using multi-temporal Landsat data employing the End Point Rate (EPR) and
63 Net Shoreline Movement (NSM) methods (Himmelstoss et al., 2021) and LULC changes. A
64 relationship between LULC changes and vital socioeconomic factors such as population
65 dynamics, tourism trends, and the Gross State Domestic Product (GSDP) is established to
66 assess the potential future impacts of tsunamis in the region. The results would provide
67 actionable insights to the policymakers, coastal planners, and stakeholders in disaster
68 management and sustainable coastal development.

69 **2. Study Area**

70 South Andaman region, with ~1,262 km² area and a 413 km coastline, is the
71 southernmost island of the Great Andaman, where most of the Andaman Island's population
72 and infrastructure are centered. As per the 2011 Indian census, South Andaman has a
73 population of 238,142 people, which increased to 266,900 in 2021 (estimate based on
74 www.census2011.co.in). The most habitable areas in the eastern part of South Andaman are
75 located on low lands at bay heads in addition to the higher slopes bordering bays and coastal
76 flat lands (Ghosh et al., 2004), which experienced devastation and losses during the 2004
77 Tsunami (Fig. 1). We selected 13 locations, namely South Point in Port Blair, Rutland Island,
78 Corbyn's Cove Beach, Madhuban Bay, Brichgunj, Chidiyatopu, Thirupatti Temple,
79 Wandoorjetty, Bamboo Flat, Potatang, Shoal Bay, Radha Nagar, and Govinda Nagar (Fig. 1)
80 for vulnerability assessment in the present study.



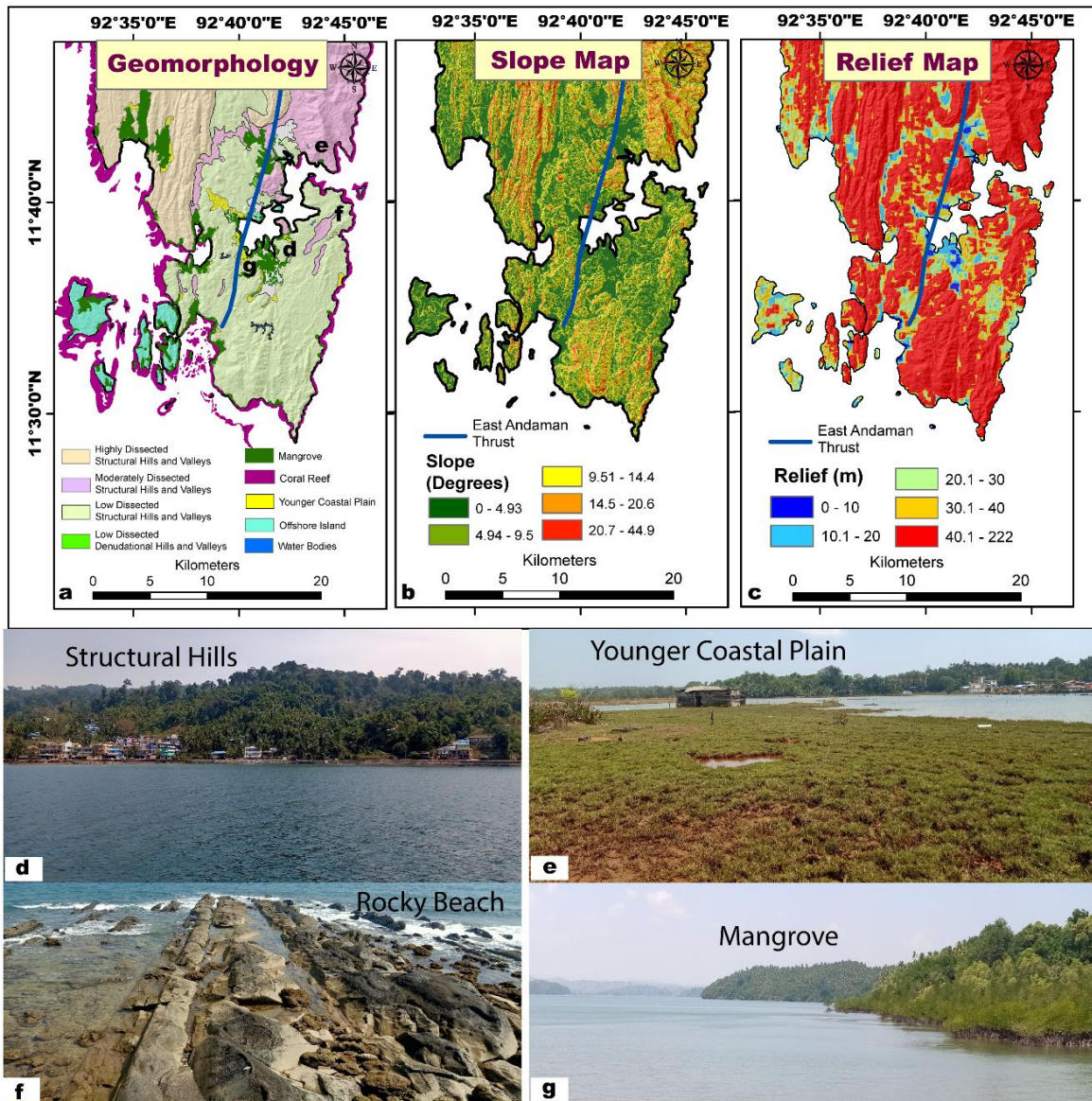
81

82 *Figure 1 Location Map of the South Andaman Region (© Google Maps & © Google Earth).*

83 The tectonic activity and weathering processes have influenced the region's topography
 84 growth and evolution (Curray, 2005; Bandopadhyay and Carter, 2017). The East Andaman
 85 Thrust, also called East Boundary Thrust, is a linear/curvilinear ~500 km long fault zone and
 86 is the locus of ongoing convergent and crustal deformation along the Sunda-Andaman plate
 87 boundary. This structure is pivotal in creating accretionary prisms within the outer-arc ridge of
 88 the Andaman and Nicobar subduction zones (Fig. 1; Bhat et al., 2023).

89 The structure-bound major geomorphological features in South Andaman include hills,
 90 valleys, beaches, mangroves, and coral reefs (Fig. 2a). The highest peak on the island is Mount
 91 Harriet, with approximately 1,200 m (3,937 feet) (southandaman.nic.in). The north-western
 92 and north-eastern parts of South Andaman are highly and moderately dissected, whereas the
 93 Southern part has low dissected structural hills and valleys (Fig. 2a, b, c, and d). The upper

94 slopes of the region are covered with high dissected structural hills with dense pristine forest
95 (Fig. 2a). The slope ranges between 0 to 44.9 degrees, with lower slopes in the coastal region
96 mostly inhabited and undergoing rapid coastline modification and Land Use Change. The
97 North, Northeast, and Southern portions of South Andaman have the steepest slope and relief
98 area, while the Eastern, Southeastern, and western parts have relatively lower slopes (Fig. 2b
99 and c). The island has a rough coastline with various bays, inlets, and headlands (Fig. 2). The
100 Younger coastal plain is a relatively flat and low-lying area adjacent to the coastline, which is
101 formed through the accumulation of sediments brought by the ocean (Fig. 2e). A wave-cut
102 platform, formed by the erosive action of waves, are flat or gently sloping rock surface are
103 found along South Point coastlines in Port Blair (Fig. 2f). These platforms can be exposed at
104 low tide, which gradually wear away the rock over time, are unique feature of rocky coastlines.
105 Coral reefs along the coast contribute to the formation of sandy beaches and barrier islands
106 (Reguero et al., 2018). Mangrove forests are found on coasts in South Andaman Island,
107 primarily in the salty water and muddy sediments lagoons and tidal zone (Fig. 2g). Mangroves
108 are crucial in stabilizing coastal ecosystems and providing habitat for various species.
109 Wandoor, Chidya tapu, and Sippighat are some notable locations of mangrove forests in South
110 Andaman coastal areas. The coastal plains in south Andaman are dynamic and prone to
111 tsunamis due to their location and active plate boundary. Therefore, studying shoreline change
112 and LULC change is especially important because of the potential impacts on local
113 communities and ecosystems.



114

115 **Figure 2 (a) Geomorphology, (b) Slope map, (c) Relief Map, (d) Structural Hills, (e) the younger coastal plain, (f)**
 116 **Rocky Beach with a wave-cut platform near south point, Port Blair, (g) Mangrove.**

117

118 3. Materials and Methods

119 It is imperative to generate a spatial dataset that may have a bearing on the dynamic changes
 120 to assess the vulnerability.

121 3.1 Data Used

122 Landsat satellite data, such as Thematic Mapper (TM) and Operational Land Imagery
 123 (OLI) sensor for the years 2004, 2005, and 2022, is used to analyze shoreline and monitor the
 124 LULC changes along the South Andaman coast in the present study. The Shuttle Radar

125 Topography Mission (SRTM) Digital Elevation Model (DEM) is used to prepare the study
 126 area's slope and relief map. We used the General Bathymetry Chart of the Ocean (GEBCO) for
 127 run-up and inundation studies along the south Andaman coastal areas (Table 1).

128 Table 1: Data used in the present study region

Data	Purpose	Date & Year	Resolution	Sources
GEBCO bathymetry	Inundation and Run-Up	2022	90 m	GEBCO (https://www.gebco.net/)
Landsat 5 TM, Landsat 8 OLI	LULC and Shoreline Change Analysis	26-02-2004 27-01-2005 27-02-2022	30 m	USGS Earth Explorer
SRTM DEM	Slope, Relief	-	30m	USGS Earth Explorer
Geomorphology	Geomorphology	-	1:250k	bhukosh.gsi.gov.in
Socioeconomic data	Population, Tourism, Gross State Domestic Product (GSDP)	1991-2021 2001-2020	-	(censusindia.gov.in) (Directorate of economics and statistics) (Rbi.org.in)

129

130 3.2 Tsunami Modeling

131 Several attempts have been made to model tsunamis to calculate inundation and determine run-
 132 up heights to evaluate their impact and hazards along mainland Indian coastal areas and
 133 elsewhere (Cho et al. 2008; Srivastava et al., 2021; Sugawara, 2021; Dani et al. 2023).

134 3.2.1 Tsunamigenic source

135 Mansinha and Smylie (1971) and Okada (1985) derived closed-form expressions for
 136 the stress and strain field at the source location for different source mechanisms. The focal
 137 mechanism and fault parameters like strike angle, dip angle, slip, and focal depth are necessary
 138 to compute the initial deformation at the source at t=0 sec (Ioualalen (2007), Rani et al. (2011),
 139 Mishra et al. (2014), and Srivastava et al. (2021)). The December 26, 2004, Sumatra earthquake
 140 of magnitude 9.3 had ruptured almost 1400 km. The region is known to have ruptured into five
 141 segments with different slip distributions. Other great tsunamigenic earthquakes in the

142 Andaman region are the 1881-Car Nicobar and the 26 June, 1941-North Andaman earthquakes
 143 (Table 2).

144 Table 2: Tsunamigenic earthquake deformation parameters used to simulate different scenarios
 145 a) 1881-Car Nicobar, and b) 1941-North Andaman earthquakes (Mishra et al., 2014), and c)
 146 2004-Sumatra (Ioualalen, 2007).

	1881-Car Nicobar	1941 -North Andaman	2004 Sumatra Earthquake				
Input Parameters			Seg1	Seg2	Seg3	Seg 4	Seg5
Longitude (DD)	92.43	92.5	94.57	93.90	93.21	92.60	92.87
Latitude (DD)	8.52	12.1	3.83	5.22	7.41	9.70	11.70
Focal Depth (km)	15	30	25	25	25	25	25
Strike angle (°)	350	20	323	348	338	356	10
Rake (°)	90	90	90	90	90	90	90
Slip (m)	5	5	18	23	12	12	12
Fault Length (km)	200	200	220	150	390	150	350
Fault Width (km)	80	80	130	130	125	95	95
Dip (°)	25	20	12	12	12	12	12
Magnitude (Mw)	7.9	7.7	9.3				

147

148 3.2.2 Tsunami wave propagation

149 The Tohoku University's Numerical Analysis Model for the Investigation of Near field
 150 tsunamis (TUNAMI-N2) to simulate the tsunami run-ups and impact using explicit leap-frog
 151 finite-difference methods by solving nonlinear shallow water wave equations, incorporating
 152 bathymetry, earthquake source parameters, and fault geometry (Imamura and Imteaz, 1995;
 153 Imamura, 1996; Goto, 1996; Imamura et al., 2006; Yalciner et al., 2003). The 2-dimensional
 154 governing equations for tsunami modeling are:

$$155 \quad \frac{\partial \eta}{\partial t} + \frac{\partial M}{\partial x} + \frac{\partial N}{\partial y} = 0$$

$$156 \quad \frac{\partial M}{\partial t} + \frac{\partial}{\partial x} \left(\frac{M^2}{D} \right) + \frac{\partial}{\partial y} \left(\frac{MN}{D} \right) + gD \frac{\partial \eta}{\partial x} + \frac{gn^2}{D^{7/3}} M \sqrt{M^2 + N^2} = 0$$

$$157 \quad \frac{\partial N}{\partial t} + \frac{\partial}{\partial x} \left(\frac{MN}{D} \right) + \frac{\partial}{\partial y} \left(\frac{N^2}{D} \right) + gD \frac{\partial \eta}{\partial y} + \frac{gn^2}{D^{7/3}} N \sqrt{M^2 + N^2} = 0 \quad (1)$$

158 In the equation-1, D is the total water depth given by $h+\eta$, τ_x , and τ_y the bottom frictions
 159 in the x- and y- directions, A the horizontal eddy viscosity which is a constant in space, and the
 160 shear stress on a surface wave is neglected. M and N are the discharge fluxes in the x- and y-
 161 directions which are given by

$$162 \quad M = \int_{-h}^{\eta} u dz = u(h + \eta) = uD \quad N = \int_{-h}^{\eta} v dz = v(h + \eta) = vD \quad (2)$$

163 The bottom friction is generally expressed as follows

$$164 \quad \frac{\tau_x}{\rho} = \frac{1}{2g} \frac{f}{D^2} M \sqrt{M^2 + N^2} \quad \frac{\tau_y}{\rho} = \frac{1}{2g} \frac{f}{D^2} N \sqrt{M^2 + N^2} \quad (3)$$

165 The friction coefficient ‘ f ’ and Manning's roughness ‘ n ’ are related by

$$166 \quad n = \sqrt{\frac{fD^{1/3}}{2g}} \quad (4)$$

167 It is seen that when D is small and f becomes large then n remains almost a constant.
 168 Substituting M , N , and the above values in fundamental equations of TUNAMI N2 are obtained
 169 which are used to solve the wave propagation using the explicit Leap-Frog finite difference
 170 Scheme as Given by Imamura, (2006).

171 3.2.3 Computational grid

172 In deep-sea regions with longer wavelengths, a coarse grid spacing to model linear effects
 173 is sufficient to resolve the wave with minimal error. As the tsunami wave propagates from deep
 174 to shallow waters, the wavelength shortens and the amplitude increases, it follows a non-linear
 175 pattern of amplitude dispersion, energy dissipation, and bottom friction and requires finer
 176 resolution grids with more node points to accurately capture the wave dynamics and minimize
 177 errors. The grid spacing should follow the Courant-Friedrich-Lewy conditions for checking the

178 convergence of the numerical code to a certain asymptotic limit using the following
179 relationship,

$$180 \quad \Delta x / \Delta t = \sqrt{2gh_{\max}} \quad (5)$$

181 Where Δt and Δx are temporal and spatial grid sizes, h_{\max} maximum still water depth in the
182 computational domain, and g is the gravitational acceleration.

183 To observe the non-linear or near-shore effects of a tsunami a high-resolution
184 bathymetry and topography is considered. In the present study, we used GEBCO bathymetry
185 and topography data formatted into four grids of 81, 27, 9, and 3arc seconds resolutions at a
186 spacing ratio of 1:3 for grids A, B, C, and D, respectively (Fig. S1). In most computations, the
187 manning coefficient is around 0.025 as it consists of gravel and sand (Masaya et al., 2020);
188 however, different manning coefficients can be considered for rough bathymetry (Dao and
189 Tkalich, 2007). A value of 0.01 is considered for smooth bathymetry and stony cobbles, and a
190 roughness of 0.035 can be considered. The viscosity and roughness have a certain influence on
191 mild slopes but it is negligible for steep slopes and a dynamic friction coefficient from 0.01 to
192 0.1 can be considered (Zhang et al., 2024). For the propagation of tsunamis in shallow water,
193 the horizontal eddy turbulence terms are negligible as compared with the bottom friction (Dao
194 and Tkalich, 2007) We simulate the tsunami waves using the TUNAMI-N2 code to get the
195 directivity map, the wave amplitudes (run-up heights), and inundation distance at different
196 locations in the study region.

197 **3.3 Shoreline Analysis in DSAS**

198 The USGS's digital shoreline analysis system (DSAS) version 5.1 (an ArcGIS
199 extension) estimates shoreline changes. The procedures are executed in 4 steps: shoreline
200 digitization, baseline generation, transect generation, and computation of the shoreline change
201 rate (Raj et al., 2020; Natarajan et al., 2021). The digitized shorelines for 2004, 2005, and 2022

202 years have been added to a personal geodatabase in a single shapefile. The shoreline image
203 data is added to the attributes as MM/DD/YYYY, and the baseline is in the meter UTM
204 projected coordinate system. To estimate rates of change, DSAS uses baseline measurements
205 of a time series of shorelines and a shapefile (Leatherman, 2003). Generating transects involves
206 initially choosing a predefined set of parameters from the personal geodatabase, including
207 settings for the baseline and shoreline. Subsequently, we placed these transects perpendicular
208 to the shoreline, extending 800 m at intervals of 150 m along the entire shoreline, originating
209 from the baseline. A 50 m smoothing distance was applied using the 'cast transects' tool within
210 DSAS to ensure a smoother outcome.

211 The evaluation of uncertainty encompasses natural and anthropogenic forces such as
212 wind, waves, tides, currents, and human influences, along with the accuracy of measurement
213 techniques, including digitization, interpretation, and GPS error. The accuracy of shoreline
214 position and the rates of shoreline change can be influenced by various error sources, such as
215 the position of the tidal level, image resolution, digitization error, and image registration
216 (Jayson-Quashigah et al., 2013; Vu et al., 2020, Basheer et al., 2022). Therefore, the shoreline
217 positional error (E_a) for each transect was calculated using Equation (6):

218

$$219 \quad E_s = \pm \sqrt{E_s^2 + E_w^2 + E_d^2 + E_r^2 + E_p^2} \quad (6)$$

220 Where E_s is the seasonal error due to seasonal shoreline fluctuations, which is $\sim \pm 5$ m in
221 extreme ocean level (EOL); E_w is the tidal error, E_d is the digitization error, E_r is the
222 rectification error and E_p is the pixel error (Fletcher et al. 2011; Vu et al., 2021). This
223 approach assumes that the component errors are normally distributed (Dar & Dar, 2009).
224 The total uncertainties were used as weights in the shoreline change calculations. The

225 values were annualized to provide errors (E_u) estimation for the shoreline change rate at
226 any given transect, expressed in Equation (7):

$$227 \quad E_u = \pm \frac{\sqrt{U_{t_1}^2 + U_{t_2}^2 + U_{t_3}^2 + U_{t_4}^2 + U_{t_n}^2}}{T} \quad (7)$$

228 where t_1 , t_2 , and t_n are the total shoreline position error for the various years and T is the
229 years of analysis.

230 The uncertainty in the shoreline analysis is due to the influence of tides on the Landsat
231 satellite imagery, which is minuscule in the extensive coastline of the study area. We used
232 monthly tide gauge data from the Permanent Service for Mean Sea Level (PSMSL) database
233 (<https://psmsl.org/data/obtaining/stations/206.php>) at Port Blair station for 2003-2004 and
234 2017-2021. The data for 2004-2005 and 2022 are unavailable. The tide excursion of 383 mm
235 or 0.383 m (Fig. S2) is estimated from the highest (1100 mm) and lowest (717 mm) tide gauge
236 measurements recorded between 2017 and 2020. We calculated uncertainty of 7.21m and
237 7.12m for 2018-2019 and 2019-2020, respectively, and the same is adopted for 2022 owing to
238 similar ranges (Table S1). The mean slope of the shore areas is 4-12 degrees near 7 zones. (Fig.
239 S3, Table S2). We used End Point Rate (EPR) and Net Shoreline Movement (NSM) methods
240 to analyze the shoreline change (Himmelstoss et al., 2021). To quantify uncertainty, a
241 confidence interval of 90% and a shoreline uncertainty value of 10m were adopted based on
242 the recommendations of the United States Geological Survey (USGS) under the National
243 Assessment of Shoreline Change project (Himmelstoss et al., 2021; Den and Oele, 2018 and
244 Joesidawati, 2016).

245 **3.3.1 Net Shoreline Movement (NSM)**

246 NSM is used to determine the net change in the shoreline position over a specific period by
247 finding the perpendicular distance between the most recent shoreline (in this case, 2022) and
248 the oldest shoreline (2004) along each transect. The formula for NSM can be expressed as:

249
$$\text{NSM} = \{d_{2022} - d_{2004}\}m$$

250 **3.3.2 End Point Rate (EPR)**

251 EPR quantifies the shoreline change rate over time and is calculated by dividing the Net
252 Shoreline Movement (NSM) by the time elapsed between the oldest and most recent shoreline
253 measurements, which indicates the rate of erosion or accretion. It is important to have data
254 from at least two shoreline dates (Dolan et al., 1991; Crowell et al., 1997). The formula for
255 EPR can be expressed as follows:

256
$$\text{EPR} = \left\{ \frac{d_{2022} - d_{2004}}{t_{2022} - t_{2004}} \right\}$$

257 **3.4 Land Use Land Cover Analysis (LULC)**

258 The LULC map uses Landsat 5 TM (2004 and 2005) and Landsat 8 OLI (2022). False Colour
259 Composite (FCC) satellite images combine near-infrared, red, and green bands to delineate five
260 classes: Forest, built-up, Cropland, Water bodies, and Inundated areas. (Prabhbir and Kamlesh,
261 2011). Tone, texture, size, shape, pattern, association, and other visual interpretation techniques
262 also were used to interpret different land use classes. Maximum likelihood is a supervised
263 classification method used in this study to detect LULC change. Each pixel in the classified
264 Landsat images varies over time due to changes in land cover.

265 **4. Results**

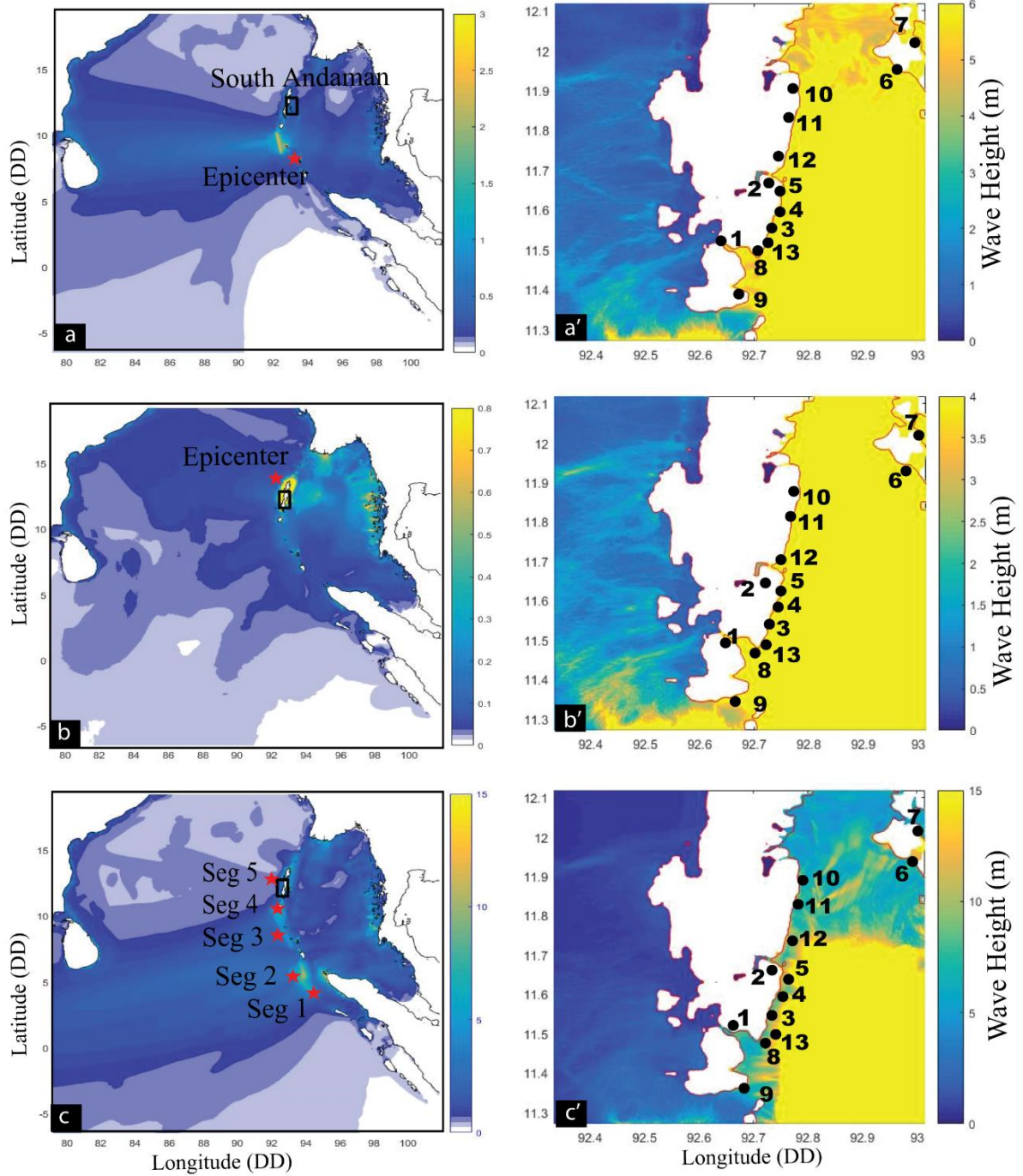
266 An analysis of the 2004 tsunamigenic earthquake's impact on the South Andaman
267 region, focusing on tsunami directivity, arrival times, run-up heights, shoreline changes, and
268 LULC impact, is examined in detail.

269 **4.1 Tsunami studies along the South Andaman Region**

270 We have considered three tsunamigenic seismic scenarios, namely, a) the 1881-Car
271 Nicobar earthquake, b) the 1941-North Andaman earthquake, and c) the 2004 Sumatra
272 earthquake, and generated the directivity and run-up maps(Fig. 3). The directivity map shows

273 that most of the energy propagation is in the East-West direction (Fig. 3 a,b,c), and the
274 shallower waters surrounding the Andaman and Nicobar Islands has significance influence on
275 the east-west propagation of tsunamis (Singh et al., 2012). The run-up height along the eastern
276 coast of South Andaman is greater than the western coast (Fig. 3 b', c', d'; Table 3). This
277 difference is due to the wider continental shelf on the Western coast of the south Andaman
278 region and shallow water depths. In the case of a higher magnitude of tsunamigenic earthquakes
279 in the Car Nicobar or the North Andaman region, higher run-ups will be observed along the
280 locations, which are considered for the present study (Table 3).

281 The arrival times of tsunamis vary from 21 minutes to 58 minutes across different locations for
282 these earthquakes, with the 1881-Car Nicobar earthquake generally resulting in the shortest
283 arrival time (Fig. 3; Table 3). The run-up heights range from 1-13 m at different locations (Fig.
284 3; Table 3), which are resultant of earthquake magnitude, the source's proximity to observation
285 locations, and the local coastal topography that also affected inundations. The extent of
286 inundation, representing the area covered by the tsunami, ranges from 10m to 950m, with a
287 wide variation across locations and earthquake events. The 2004 Andaman Sumatra earthquake
288 resulted in higher run-up heights and inundations compared to the 1881 Car Nicobar, and 1941
289 Andaman earthquakes and caused extensive damage. Hence, we considered the 2004-
290 Andaman Sumatra earthquake for a detailed analysis of hazard assessment and scenario
291 analysis. The arrival times (minutes), run-up height (meter), and inundation extent (meter) at
292 13 different locations along the South Andaman region for the 2004 Sumatra earthquake (Table
293 3) are considered for further analysis.



294

295 *Figure 3: (a) Directivity and (a') wave run-up height for the 1881-Car Nicobar, (b and b') for the 1941-Andaman,*
 296 *and (c and c') for the 2004-Sumatra earthquakes.*

297

298

299 Table 3: Estimated Arrival times, Run-up heights, and inundations at the studied locations from
 300 tsunamigenic a) 1881-Car Nicobar, b)1941-North Andaman earthquakes, and c) 2004-Sumatra
 301 earthquake sources. The SN of locations is common for Figs. 3 and 4.

SN	Gauge Locations	Longitude Latitude (DD)	Earthquake Sources	Arrival Time (Min.)	Run-up (m)	Inundation (m)
1	Wandoorjetty	92.614750, 11.581667	a) 1941-North Andaman	22.5	1.25	180
			b) 1881 Car Nicobar	32.80	2.21	200
			c) 2004 - Sumatra	36.5	3.5	450
2	Bombooflat	92.715417, 11.700722	a) 1941-North Andaman	24.55	2.23	350
			b) 1881 Car Nicobar	31.2	2.35	650
			c) 2004 - Sumatra	42	5.5	90
3	Corbyns Cove Beach	92.770916, 11.642372	a) 1941-North Andaman	22.3	2.1	320
			b) 1881 Car Nicobar	28.8	2.3	580
			c) 2004 - Sumatra	33	12.7	900
4	South Point, Port Blair	92.702917, 11.652389	a) 1941-North Andaman	22	2.12	280
			b) 1881 Car Nicobar	28.4	2.31	500
			c) 2004 - Sumatra	31.5	9.6	550
5	Thirupatti Temple	92.703861, 11.581694	a) 1941-North Andaman	21.75	1.42	360
			b) 1881 Car Nicobar	46.5	1.65	400
			c) 2004 - Sumatra	38	1	200
6	Radha Nagar	92.951722, 11.979306	a) 1941-North Andaman	52	2.1	180
			b) 1881 Car Nicobar	54	3.8	220
			c) 2004 - Sumatra	54	2.6	156
7	Govinda Nagar	92.989139, 12.030167	a) 1941-North Andaman	56	1.8	220
			b) 1881 Car Nicobar	58	3.2	190
			c) 2004 - Sumatra	58	3.6	195
8	Chidiyatopu	92.716639, 11.499306	a) 1941-North Andaman	21.75	1.79	300
			b) 1881 Car Nicobar	26.5	2.05	500
			c) 2004 - Sumatra	36	3.9	585
9	Rutland Island	92.703818, 11.431497	a) 1941-North Andaman	25.9	1.01	585
			b) 1881 Car Nicobar	26.55	1.44	380
			c) 2004 - Sumatra	27	6	700
10	Shoal Bay	92.795963, 11.934202	a) 1941-North Andaman	34.8	1.77	180
			b) 1881 Car Nicobar	42.5	1.45	220
			c) 2004 - Sumatra	56	13	950
11	Potatang	92.801282, 12.027380	a) 1941-North Andaman	36	1.5	200
			b) 1881 Car Nicobar	46	1.4	180
			c) 2004 - Sumatra	58	12.5	210
12	Madhuban Bay	92.785534, 11.782775	a) 1941-North Andaman	32	1.9	180
			b) 1881 Car Nicobar	40	1.5	200
			c) 2004 - Sumatra	54	6.9	210
13	Brichgunj	92.770162, 11.618980	a) 1941-North Andaman	28	1.3	200
			b) 1881 Car Nicobar	32	4	300
			c) 2004 - Sumatra	30	10	585

303 Due to the effects of the 2004 tsunami, the stagnation of tsunami water in the
304 agricultural lands and low-lying areas of the Wandoor region resulted in increased soil salinity
305 (Fig. 4a); it also damaged the bridge in the Bombooflat area (Fig. 4b), and houses near the
306 Sippighat area (Fig. 4c, d). Shoal Bay recorded the highest inundation extent of 950m and
307 experienced the highest run-up height of 13m, indicating significant wave impact (Fig. 3b;
308 Table 3). Corbyn's Cove Beach and Rutland Island experienced significant inundation
309 distances exceeding 700m (Fig.3b, Table 3). Potatang, Corbyns Cove Beach, and Brichgunj
310 also recorded relatively high run-up heights that exceeded 9m (Table 3). Most locations
311 experienced arrival times between 27 and 58 minutes, indicating a relatively quick propagation
312 of the tsunami wave. Jain et al. (2005) mentioned that tsunami waves arrived between 40 and
313 50 minutes in the Andaman and Nicobar Islands. Our results agree with the tsunami run-up
314 heights estimation by Cho et al. (2008) and Prerna et al. (2015) at a few locations in the present
315 study area. Since the tide gauge data are available at a few locations along the Indian coast, we
316 rely on limited field observations along the coast to validate our findings. The field
317 observations of the water marks on a light post at Bambooflat in Port Blair. was seen to be
318 around 3.8m (Cho et al., 2008) and our computations show it to be ~ 3.5m, which is within
319 ~7% error limit. Similarly at South Point, Port Blair, the field observations are 10m, and our
320 computations value is 9.6m, which is ~4% deviation and the deviation is 7% at Chidiyatopu.
321 The Bambooflat region and Harbour area of Port Blair experienced liquefaction affecting
322 several buildings (Murty et al., 2006), our computations have shown that the tsunami wave
323 heights were around 5.5m. At most locations, the computed values are within 10% error.

324 South Andaman experienced significant inundations during the 2004 Sumatra
325 earthquake, highlighting the urgent need for robust mitigation and preparedness measures in
326 these vulnerable coastal regions. We aim to contribute to this broader goal by providing
327 essential data and insights to support evidence-based decision-making and mitigate the adverse

328 impacts of tsunamis on coastal populations. The study will provide workable input to the local
 329 risk management strategies involving local communities, optimizing evacuation planning,
 330 enhancing early warning systems, fortifying infrastructure resilience, and adopting a multi-
 331 hazard risk assessment approach (National Research Council, 2011).

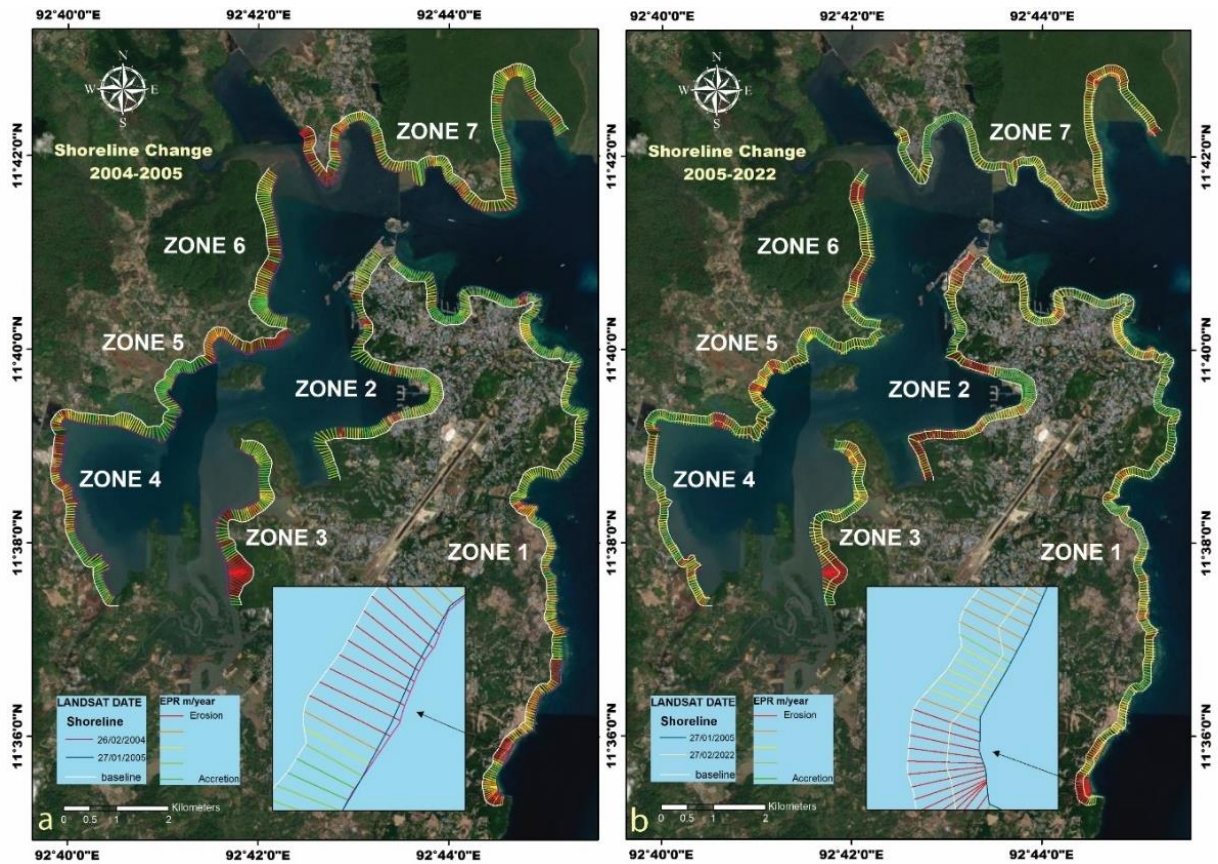


332
 333 *Figure 4: (a) Stagnation of Tsunami water in the agricultural field and Low-laying areas in Port Blair, (b) damaged*
 334 *bridge in Bombooflat, (c, d) damaged house in the Sippighat area near Port Blair (Photo: 01/03/2023). The*
 335 *number on the field photograph corresponds to respective locations as in Fig. 3.*

336 4.2 Shoreline Change during Tsunami (2004-2005) and post-tsunami (2005-2022)

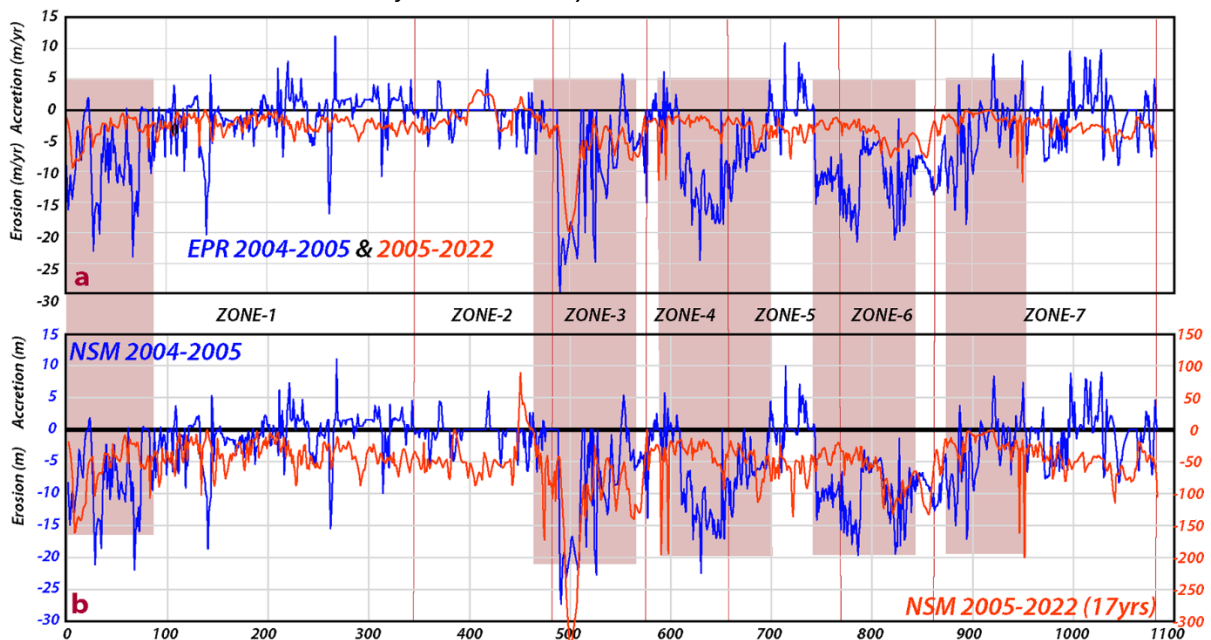
337 The south Andaman coasts are divided into seven zones based on proximity with the
 338 inundation studies to calculate NSM and EPR to understand the short-term and long-term
 339 changes impact of coastal erosion (Fig. 5, Supplement Fig. S4-S10). The NSM and EPR are
 340 calculated over two separate time frames to comprehend the damages caused by tsunamigenic
 341 and regular wind-wave-surge events in South Andaman Island. These zones were used to
 342 understand erosion and accretion rates between (i) 2004 - 2005 (Fig. 5a) and (ii) 2005-2022
 343 (Fig. 5b). The EPR and NSM values from 2004 to 2005 indicate the direct effect of tsunami

344 waves, whereas 2005 to 2022 values represent periodic wind-wave-surge dynamics. Periodic
345 coastal shoreline changes refer to the regular and repeating fluctuations in the position of the
346 shoreline along the coast. Natural and human-induced factors can influence these changes. A
347 total of 1,083 transects are created at 50-m intervals, distributed among the zones as follows:
348 Zone 1 (339 transects), Zone 2 (147 transects), Zone 3 (89 transects), Zone 4 (74 transects),
349 Zone 5 (137 transects), Zone 6 (73 transects), and Zone 7 (220 transects). The shoreline
350 variation rates indicate positive accretion and negative erosion (Fig. 6, Table 4). The EPR
351 Changes in meters per year (m/y) for the periods 2004-2005 show a higher erosion rate
352 compared to 2005-2022, particularly in Zones 3, 4, and 5 (Fig. 6a). The NSM focused on two
353 distinct time frames, indicate the NSM rates during the tsunami, for the year of 2004-2005, and
354 the NSM rates over the extended 17-year period from 2005 to 2022 are measured in meters
355 (Fig. 6b). The detailed analysis of the maximum (accretion), minimum (erosion), and mean
356 shoreline changes for each of the seven zones that occurred during the tsunami event and the
357 post-tsunami period are discussed below.



358

359 Figure 5: Shoreline changes observed (a) during 2004-05 due to the tsunamigenic process and (b) from 2005-
 360 2022 due to wind wave surges overlaid on Google Earth images (@Google Earth). The affected coastline is
 361 subdivided into seven distinct zones for detailed analysis.



362

363 Figure 6: (a) The rates of erosion and accretion in seven distinct Zones along the South Andaman shoreline using
 364 EPR methods, and (b) NSM have been conducted between the years 2004-2005 and 2005-2022. Highlighted color
 365 indicating high erosion zone
 366

367 **Table 4** Shoreline change in southern Andaman is observed for 2004-2005 and 2005-2022
 368 using USGS's DSAS methods (Himmelstoss et al., 2021).

		2004-2005		2005-2022	
ZONE		EPR(m/y)	NSM(m)	EPR(m/y)	NSM (m)
ZONE 1	Mean	-2.85	-2.62	-2.55	-43.57
	Minimum	-23.9	-21.29	-9.44	-161.21
	Maximum	12.05	11.06	0	0
ZONE 2	Mean	-0.54	-0.50	-1.0639	-18.174
	Minimum	-7.17	-6.58	-4.56	-77.93
	Maximum	6.54	6	3.25	55.56
ZONE 3	Mean	-9.92	-8.11	-7.10	-121.51
	Minimum	-24.71	-23.27	-19.87	-339.51
	Maximum	5.58	4.37	-1.02	-17.42
ZONE 4	Mean	-7.92	-7.72	-2.24	-38.34
	Minimum	-24.47	-22.46	-11.42	-195.03
	Maximum	6.23	5.72	-0.79	-13.42
ZONE 5	Mean	-6.594	-6.05	-2.94	-50.26
	Minimum	-21.47	-19.7	-7.95	-135.83
	Maximum	10.88	9.99	-1.03	-17.54
ZONE 6	Mean	-9.74	-8.94	-4.92	-84.05
	Minimum	-21.18	-19.44	-7.75	-132.39
	Maximum	-1.46	-1.34	-1.86	-31.73
ZONE 7	Mean	-2.16	-1.986	-2.43	-41.56
	Minimum	-18.65	-17.29	-11.7	-199.96
	Maximum	9.77	8.97	-0.04	-0.61

369
 370 ZONE 1: This zone experienced a combination of erosion and accretion between 2004-05 and
 371 2005-21. The maximum erosion rates are observed at Megapoda, with an EPR of -23.9
 372 m/y. and -9.44 m/y., NSM analysis shows the estimated erosion is -21.29m and -161.21m
 373 respectively (Fig. S4 a, b, Table 4). The southern part of South Andaman Island has more
 374 shoreline erosion rather than accretion, which can be attributed to the heightened impact
 375 of tsunamis on the southern region, a phenomenon that is more significant when
 376 compared to the northern part of South Andaman Island. These Sediments eroded from
 377 one coastline area are often transported along the shoreline by the longshore currents.
 378 The angle of wave approach creates these currents and is responsible for moving
 379 sediment parallel to the coastline.

380 ZONE 2: This zone experienced a combination of erosion and accretion between 2004-05 and
 381 2005-21. The maximum rate of erosion is -7.17 m/y and -4.56 m/y (EPR) was recorded

382 at IOC Colony, while the maximum accretion rate of 6.54 m/y and 3.25 m/y (EPR) was
383 observed at Ashwin Nagar Respectively. The NSM analysis indicated a shoreline retreat
384 of -6.58 m at IOC Colony and -77.93 m advancement at Ashwin Nagar. The jetties in the
385 Jungli Ghat port played a role in controlling erosion and accretion at these sites (Fig. S5,
386 Table 4).

387 ZONE 3: This zone experienced a combination of erosion and accretion between 2004-05 and
388 2005-21. The maximum erosion rate is -24.71 m/y and -19.87 (EPR) at Flat Bay, while
389 the maximum accretion rate is 5.58 m/y and (EPR) at NLC Limited. The NSM analysis
390 revealed a shoreline retreat of -23.27 m and -339.51 m at Flat Bey. High wave energy
391 and exposure to strong currents, which are more common near Flat Bay, can lead to
392 increased erosion of mangrove shorelines (Fig. S6, Table 4).

393 ZONE 4: This zone experienced a combination of erosion and accretion between 2004-05 and
394 2005-21. The maximum erosion rate is -24.47 m/y at Ferrargunj and -11.24 m/y (EPR)
395 at PLK Creek Resort, NSM estimated erosion is -22.46 m and -195.03m at Chouldari
396 (Fig. S7). We observed the shoreline erosion area using the Landsat time-lapse satellite
397 images between 2004-2005, and 2022 near Flat Bay, South Andaman, has revealed
398 noteworthy environmental changes. The dark blue color observed in 2004 and 2005
399 indicates the presence of deep-water bodies, whereas the light blue color in the 2022
400 image suggests the water bodies have become shallow with significant fresh sediment
401 load (Fig. 7; Table 4).

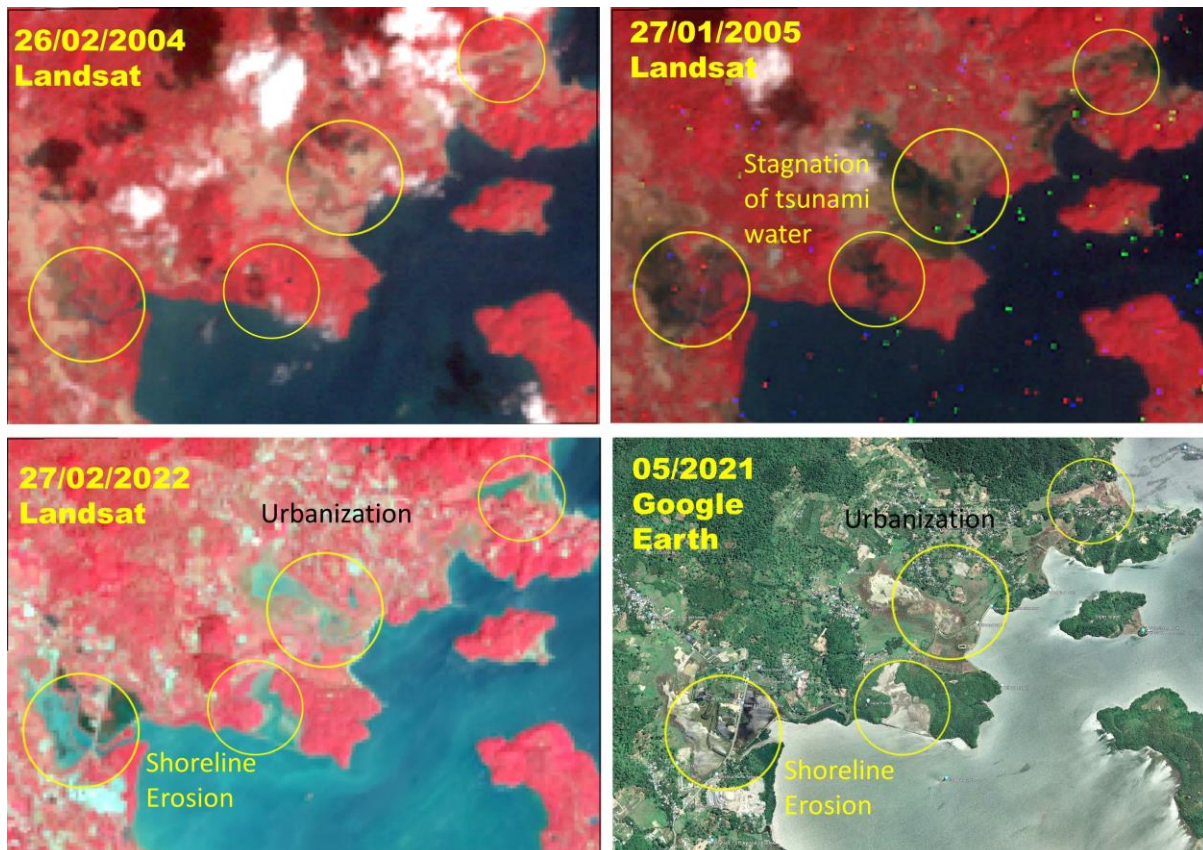
402



403

404 *Figure 7: shows a time-lapse satellite imagery of Landsat 8 FCC near the Flat Bay area (marked in yellow circle)*
 405 *during the years 2004 and 2005 showing robust mangrove coverage is evident. However, when comparing the*
 406 *Landsat 8 image in 2022 and the corresponding Google Earth image (@Google Earth), it is apparent that the*
 407 *mangrove ecosystem in this area has experienced substantial erosion and the development of Solar panels.*
 408

409 ZONE 5: The maximum erosion rate of -21.47 m/y (2004-05) and -7.95 (EPR 2005-22) is
 410 recorded at Mithakhari. According to the NSM analysis, the shoreline retreated by -19.7
 411 m and -132.39m at Mithakhari (Fig. S8). In this zone, Coastal development,
 412 infrastructure construction, and alteration of natural hydrological patterns can disrupt
 413 sediment transport and exacerbate erosion (Fig. 8; Table 4).
 414



415

416 *Figure 8: shows Landsat 8 time-lapse imagery and @ Google Earth imagery near the Ograbraj and Mithakhari*
 417 *region depicting the erosion activity during and after the tsunami and the imagery shows a significant growth in*
 418 *the built-up areas surrounding the tsunami-affected areas in 2004.*

419

420 **ZONE 6:** This zone is predominantly affected by erosion, with no observed accretion. The

421 maximum erosion rate is -21.18 m/y and -7.75 m/y (EPR) at Namunaghar, and the NSM

422 estimated erosion is -19.44 m and -132.39m at Namunaghar (Fig. S9). In February 2004,

423 immediately before the catastrophic tsunami event, there was no observable presence of

424 stagnant water in the area (Fig. 9). However, by January 2005, following the tsunami, the

425 images distinctly exhibited the stagnant water. In February 2022, the same location

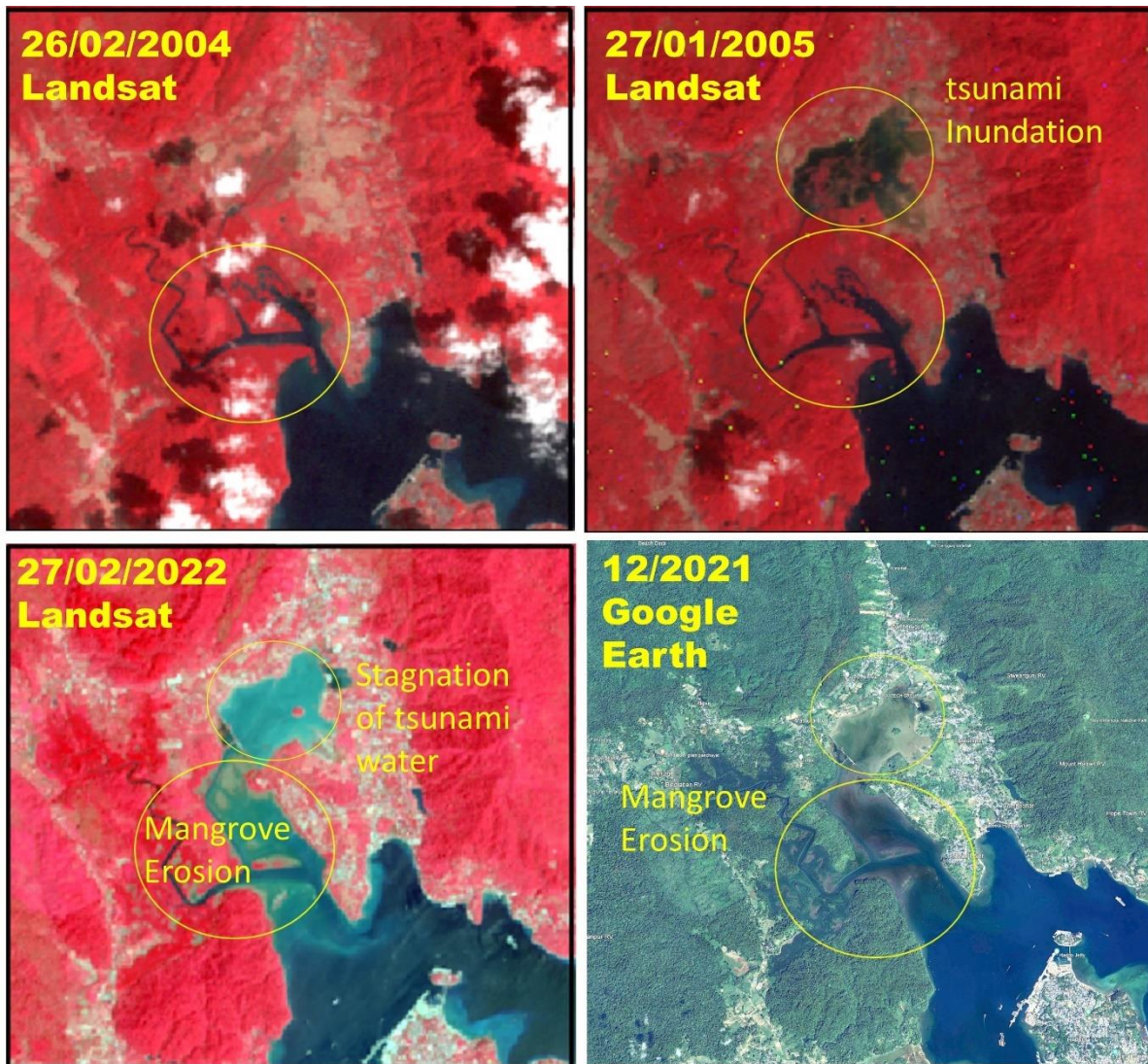
426 exhibited substantial shoreline erosion within the extensive mangrove and agricultural

427 area, accompanied by increased urban development along the shoreline. The progression

428 of urban development was also validated using Google satellite imagery. The sediment

429 carried by ocean currents deposited in low-lying areas revealed caused shallowing and

430 significant changes in ocean water color.



432

433 *Figure 9: shows the Change detection of the shoreline using Landsat 8 time-lapse imagery and © Google Earth*
 434 *imagery for 2004 before, 2005 after the tsunami, and the 2022 present status of the shoreline.*

435

436 **ZONE 7:** This zone experienced a combination of erosion and accretion between 2004-05 and

437 2005-21. The maximum erosion rate is -8.36 m/y and -11.7 m/y (EPR) at Shore Point,

438 while the maximum accretion rate is 9.77 m/y (EPR). The NSM analysis indicated an

439 erosion of -17.29 m at Shore Point and -199.96 m at North Bay (Fig. S10; Table 4).

440 Notably, a tsunami with a height of 9.6 m was observed at Shore Point.

441 The natural rate of shoreline movement in the South Andaman region has increased

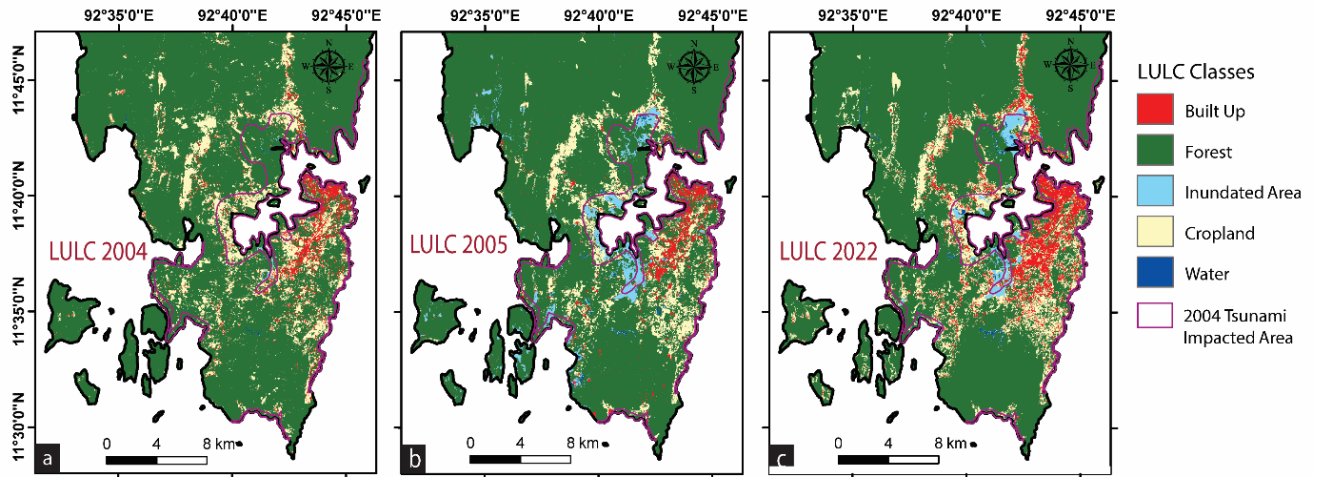
442 following the tsunami event, which is attributed to several factors, including the removal of

443 vegetation cover, the softening of exposed bedrock, and the destabilization of unconsolidated
444 materials caused by the tsunami, all of which have made the region more susceptible to erosion
445 (Yunus et al., 2016). Comparing the erosion and accretion rates suggests the erosion rates were
446 significantly less during the 2005-2022 period in comparison to the 2004-05 tsunami,
447 highlighting the adverse effect of the tsunami.

448 **4.3 Land Use and Land Cover (LULC) Analysis**

449 The LULC is categorized into 5 distinct classes: Built-up, Forest, Inundation, Cropland,
450 and water Bodies (Fig. 10). The overall accuracy obtained is 90.11%, 89.96%, and 90.30%
451 with a quantitative assessment of K_{hat} (Kappa) coefficient is 0.78, 0.762 and 0.79 for 2004, 2005
452 and 2022 images, respectively (**Table S3**). Our primary objective is to determine the extent of
453 land use pattern changes from 2004 to 2022 in areas affected by the 2004 tsunami. Several
454 researchers have already examined the vulnerability and impact of the 2004 tsunami on South
455 Andaman, including (Velmurugan et al., 2006; Debjani et al., 2012; Sachithanandam, 2014).

456 The LULC classification for the South Andaman region in tsunami-impacted areas in
457 the years 2004, 2005, and 2022 reveals significant changes (Fig. 10, Table 5). 1) The built-up
458 area decreased from ~7.38% in 2004 to 6.23% in 2005, marking a 1.15% decrease. However,
459 it subsequently increased by 11.11% by 2022. 2) Cropland coverage decreased from around
460 22.12% in 2004 to ~11.93% in 2005, indicating a substantial reduction of 10.19%. It then
461 increased to 17.15% by 2022. 3) Inundation areas increased from about 3.29% in 2004 to
462 27.65% in 2005, showing a notable rise of 24.36%. However, by 2022, they decreased by
463 ~18.57%. 4) Forested areas saw a significant decrease from ~66.46% in 2004 to about 51.10%
464 in 2005, signifying a reduction of 15.36%. This decrease persisted in 2022, remaining at
465 ~51.10%. 5) Water bodies covered around 0.62% of the area in 2004, which increased slightly
466 to about 0.76% in 2005. By 2022, there is a more significant increase, reaching 2.05%.



467

468 *Figure 10: (a) LULC 2004 (b) LULC 2005, and (c) LULC 2022 in tsunami-impacted areas (pink color) and South*
 469 *Andaman.*

470 **Table 5: LULC Analysis for 2004, 2005 to 2022 in tsunami impacted area**

LULC classes	2004 Area in km ²	2004 % of Area	2005 Area in km ²	2005 % of Area	2022 Area in km ²	2022 % of area
Built-Up	3.57	7.38	3.01	6.23	5.38	11.11
Forest	32.19	66.46	25.79	53.40	24.74	51.10
Inundation Area	1.64	3.39	13.36	27.65	8.99	18.57
Cropland	10.71	22.12	5.76	11.93	24.74	17.15
Water Bodies	0.30	0.62	0.36	0.76	0.99	2.05
Total Area (Sq. Km)	48	100	48	100	48	100

471

472 The LULC classification for the South Andaman region in the years 2004, 2005, and 2022
 473 shows significant changes (Figure 10, Table 6)

474 **1) Built-Up Area:** In 2004, the built-up area covered 19.92 km², constituting ~3.84% of the
 475 total study area. By 2005, this area had reduced to 17.66 km², accounting for 3.41% of
 476 the total area. by 2022, there was a significant expansion, with the built-up area
 477 occupying 45.07 km², representing 8.68% of the total region.

478 **2) Forest:** In 2004, forests dominated the landscape, covering 432.85 km², which was
 479 approximately 83.43% of the total study area. By 2005, this forested area slightly
 480 decreased to 420.79 km², comprising 81.27% of the total area. However, by 2022, the

481 forest cover continued to decline, with an area of 408.66 km², accounting for 78.78% of
 482 the total region.

483 **3) Inundation Area:** In 2004, the inundation area was limited, covering 3.40 km² or 0.65% of
 484 the total area. In 2005, there was a substantial increase, expanding to 28.41 km², which
 485 represented 5.48% of the total area. By 2022, the inundation area decreased to 13.89 km²,
 486 making up 2.66% of the total region.

487 **4) Cropland:** Cropland covered 61.77 km² in 2004, accounting for 11.90% of the total study
 488 area. By 2005, this area reduced to 49.34 km², representing 9.53% of the total area. In
 489 2022, the cropland area further decreased to 48.65 km², making up 9.37% of the total
 490 region.

491 **5) Water Bodies:** In 2004, water bodies covered a small area of 0.83 km², approximately 0.16%
 492 of the total area. By 2005, this area slightly increased to 1.54 km², constituting 0.29% of
 493 the total region. There was a more significant expansion during 2022, with water bodies
 494 occupying 2.45 km², accounting for 0.47% of the total area.

495 Table 6: LULC Analysis for 2004, 2005 to 2022 in the Study region

LULC	2004 Area in km ²	2004 % of Area	2005 Area in km ²	2005 % of Area	2022 Area in km ²	2022 % of area
Built-Up	19.92	3.84	17.66	3.41	45.07	8.68
Forest	432.85	83.43	420.79	81.27	408.66	78.78
Inundation Area	3.40	0.65	28.41	5.48	13.89	2.66
Cropland	61.77	11.90	49.34	9.53	48.65	9.37
Water Bodies	0.83	0.16	1.54	0.29	2.45	0.47
Total Area (Sq. Km)	518	100	518	100	518	100

496
 497 **5. Discussion**

498 The complex interaction between geomorphology, shoreline change, LULC changes, and
 499 economic factors in tsunami vulnerability and impact assessment in South Andaman is
 500 discussed below;

501 **5.1 Shoreline changes VS LULC**

502 The impact of tsunamis varies due to differences in landforms, relief, slope, elevation, and
503 the presence (or absence) of natural barriers such as coral reefs and mangroves. It has been
504 observed that for a given water depth on the shelf, if the continental slope is steeper, greater
505 mangrove cover, greater relief, and higher elevation can result in a greater amount of energy
506 being reflected, leading to a smaller tsunami wave height on the shelf. On the other hand, with
507 a flatter slope, low relief, and less vegetation cover area on the coastal side, the reduced
508 reflection and effect of shoaling can increase tsunami wave height (Siva et al., 2016). Coastal
509 erosion is a natural process in south Andaman that occurs when waves, currents, tsunamis, and
510 tides erode the shoreline, removing sediment and land over time. Factors such as sea-level rise,
511 wave energy, storm events, and human activities can contribute to increased rates of erosion.

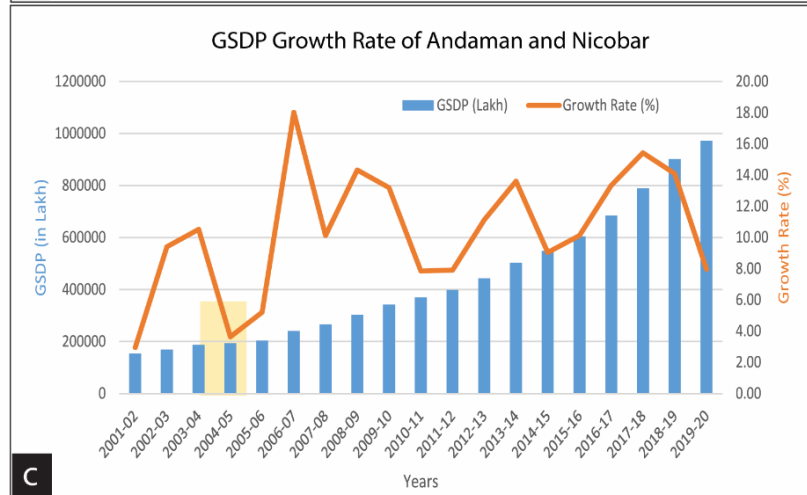
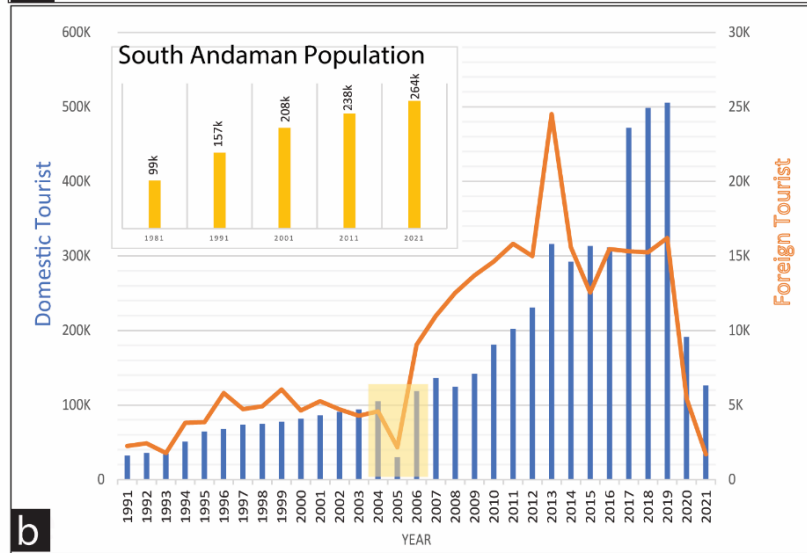
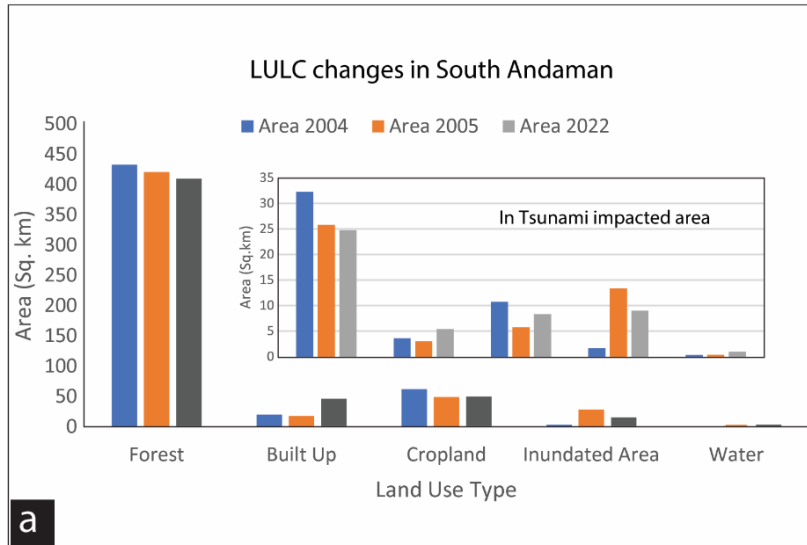
512 Over time, the geomorphological landforms continue to shape and modify the landscape.
513 However, human activities and developmental pressures are significant drivers of LULC
514 change in South Andaman (Fig. 10 a, b, c). Common LULC changes observed in the area
515 include deforestation for urban expansion, conversion of land for agriculture, infrastructure
516 development, and alterations to the coastal zone (Yuvaraj et al., 2014; Thakur et al., 2017;
517 Jaman et al., 2022). The interaction between geomorphology and LULC change is particularly
518 evident in the coastal regions of South Andaman, where coastal erosion and accretion processes
519 influence both LULC patterns and development decisions. The erosion occurring near the
520 shoreline leads to the loss of valuable land, affecting agricultural areas and forest regions (Fig.
521 7,8,9). Conversely, accretion processes can contribute to the growth of coastal areas by building
522 new landforms and influencing land use decisions in those locations (Nagabhatla et al., 2006;
523 Ali and Narayana, 2015; Mageswaran et al., 2021).

524 **5.2 Inundation and run observation**

525 Our computations have shown that the tsunami wave heights for around 5.5 m inundation 90
526 m are observed in Bombooflat (Fig.4b). Similarly, the harbor area of Port Blair has seen
527 structural failures in some building's foundations, and our computations show wave heights of
528 3.6m in that area. Chidiya Tapu, which is 25 km from Port Blair, the estimated run-up is 3.9
529 m, and the inundation is 585 m, which shows a gradual slope in the region (Fig. 2). Coming to
530 the Southpoint Magar area (Port Blair), a high run-up of 8.5 m is computed, and the inundation
531 level is 550 m. Houses located near the open sea were completely washed away. At Wandoor
532 Jetty in Port Blair, the calculated run-up is 3.46, the inundation is 450m, and the saltwater
533 intrusion was observed due to the tsunami.

534 **5.3 LULC vs economic change:**

535 The presence of people, infrastructure, or assets in a hazard-prone location is referred to
536 as exposure, and vulnerability is the degree to which a person, community, or system is
537 susceptible to the impacts of a hazard. Vulnerability is determined by physical, social,
538 economic, and environmental factors. (United Nations Office for Disaster Risk Reduction).
539 Several factors can contribute to changes in exposure, such as population growth, Industrial
540 development, and LULC change. It is anticipated that the population of the Andaman and
541 Nicobar Islands will double by 2050 (Nanda and Haub, 2007), and the islands are experiencing
542 an increasing influx of tourists. The increased population density in these regions intensifies
543 the strain on already vulnerable lands. As a result, when a disaster, such as a natural calamity,
544 occurs in these areas, it affects the tourists and has severe repercussions for the large local
545 population heavily dependent on tourism-related activities (Annan et al., 2005; Wood et al.,
546 2019; Sathiparan et al., 2020, Hamuna et al., 2019). The increases in population from 1971 to
547 2020, as well as built-up areas, are shown before and after the 2004 tsunami, and GSDP from
548 2001 to 2020 in tsunami-prone areas of South Andaman are observed in Fig. 11.



549
 550 *Figure 11: (a) LULC change in south Andaman and also in tsunami-affected areas of 2004. The LULC classification*
 551 *reveals that there has been a significant increase in built-up areas, inundated areas, and water bodies, while the*
 552 *agricultural land and vegetation have decreased. The increasing trends of tourists and local population in south*
 553 *Andaman can be seen in Fig. (b). The GSDP growth rate shows the macroeconomic impact on GSDP in 2005 due*
 554 *to the tsunami impact (c).*

555 The increase in built-up areas could also positively impact the GSDP by boosting the
556 construction and real estate sectors and providing more job opportunities in the tourism and
557 hospitality industries (Fig. 11a). The 2004 Indian Ocean tsunami significantly impacted the
558 GSDP of the Andaman and Nicobar Islands, particularly in the tourism and fisheries industries
559 (Fig 11c). According to a report by the National Institute of Disaster Management, the
560 Andaman and Nicobar Islands suffered losses amounting to INR 7.5 billion due to the 2004
561 tsunami, with damages to the tourism industry being the most significant. It is important to
562 carefully manage this growth and ensure sustainable development practices protecting both the
563 natural environment and the local population's well-being. This includes implementing
564 effective disaster preparedness measures, promoting sustainable tourism practices, and
565 balancing economic development with environmental conservation in the region.

566 **5.4 Implication for changing scenario of vulnerability**

567 India Inc. estimates that the total losses surpassed Rs 3,000 crore. Specifically, the losses in
568 Andaman & and Nicobar Islands exceeded Rs 1,000 crore as per industry estimates
569 (EconomicTimes.com). If a tsunami of similar magnitude were to occur again, the economic
570 loss would be five times as high as those experienced in 2004. After the 2004 tsunami, the
571 coastal area experienced significant development, with built-up areas expanding in already
572 affected areas from ~7.38 % in 2004 to ~11.11 % in 2022. This increase in urbanization and
573 infrastructure means that more properties, businesses, and critical facilities are now located in
574 the coastal zone. The affected region's local population grew from 208k in 2001 to 264k in
575 2021 (Figure 11b). With more people living in the coastal area, there is a higher risk of
576 casualties and a greater demand for resources and aid during and after a tsunami. The number
577 of tourists visiting the coastal area has increased significantly, from 98,000 tourists in 2001 to
578 500,000 by 2019 (Figure 11b). Tourists are generally less familiar with local hazards and
579 evacuation routes, making them more vulnerable during a tsunami. The presence of a large

580 number of tourists can add complexity to evacuation and relief efforts, potentially leading to
581 higher economic losses. The region has experienced a sharp decline in forest and cropland
582 areas. Forests act as natural buffers, helping to reduce the impact of a tsunami by absorbing
583 some of the wave energy. Additionally, the loss of cropland can disrupt the supply chain during
584 and after a disaster, affecting food availability and leading to economic losses beyond property
585 damage.

586 **6. Conclusions**

587 The South Andaman region is vulnerable to tsunamis due to its location in the seismically
588 active zone. In such an environment, tsunami preparedness and resilience are crucial. This
589 includes implementing effective early warning systems, raising public awareness, and
590 strengthening infrastructure resilience. Incorporating ecosystem-based approaches, such as
591 preserving and restoring natural coastal land, can also contribute to reducing tsunami
592 vulnerability. The South Andaman region is prone to shoreline changes due to natural processes
593 and human activities. Regular monitoring and assessing these changes is crucial to
594 understanding their impacts on coastal ecosystems and communities. Implementing
595 appropriate coastal management strategies, such as beach nourishment, dune restoration, and
596 erosion control measures, can help mitigate the negative effects of shoreline changes. It is
597 important to adopt sustainable land use practices that balance economic development with
598 resource conservation and responsible use. This involves promoting eco-friendly tourism,
599 protecting sensitive ecosystems like mangroves and coral reefs, and implementing land use
600 planning that considers the carrying capacity and vulnerability of the region. Tsunami modeling
601 along the coastal locations shall help decision-makers how to construct structures along the
602 coast. Decision makers will also be able to quantify the tsunami impact on sloping beaches,
603 Flat beaches, and areas having boulders/mangroves. Engaging local communities,
604 stakeholders, and indigenous knowledge holders in decision-making processes and promoting

605 capacity-building initiatives are critical for ensuring the sustainable development of the
606 Andaman region.

607 **Code availability**

608 No

609 **Data availability**

610 All data included in this study are available upon request by contacting the corresponding
611 author.

612 **Authors' contributions**

613 Vikas Ghadamode: Computations, Fieldwork, and Manuscript Writing.

614 K. Kumari Aruna: TUNAMI-N2 Computation and Fieldwork, Manuscript Writing

615 Anand Kumar Pandey: Manuscript Editing and Contribute Ideas and Suggestions

616 Kirti Srivastava: Paper Writing and TUNAMI-N2 Computations

617 **Competing interests / Conflicts of interest/**

618 The authors declare that they have no known conflicts of interest.

619 **Declarations**

620 The authors declare that they have no known conflicts of interest.

621 **Financial support**

622 No Funding

623 **Acknowledgements:**

624 The authors acknowledge encouragement and permission to publish from the Director, CSIR-
625 NGRI (Ref. No. NGRI/Lib/2024/Pub-51). VG acknowledges UGC, India, for SRF for
626 pursuing a PhD (Grant no.: 10/UGC-JRF/209/19-ESTT).

627

628 **References**

- 629 Ali, P. Y., & Narayana, A. C.: Short-term morphological and shoreline changes at Trinkat Island,
630 Andaman and Nicobar, India, after the 2004 tsunami. *Marine Geodesy*,38(1), 26-39,
631 <https://doi.org/10.1080/01490419.2014.908795> , 2015.
- 632 Annan, K.: *Reducing Risks from Tsunamis: Disaster and Development*. Nueva York: UNDP, 2005.
- 633 Bandopadhyay, P. C., & Carter, A.: Chapter 2 Introduction to the geography and geomorphology of the
634 Andaman–Nicobar Islands. *Geological Society, London, Memoirs*, 47(1), 9-18,
635 <https://doi.org/10.1144/M47.2>, 2017.
- 636 Basheer Ahammed, K. K., & Pandey, A. C.: Assessment and prediction of shoreline change using
637 multi-temporal satellite data and geostatistics: A case study on the eastern coast of India. *Journal*
638 *of Water and Climate Change*, 13(3), 1477-1493, 2022.
- 639 Bhat, G.R., Balaji, S. & Yousuf, M.: Tectonic geomorphology and seismic hazard of the east boundary
640 thrust in northern segment of the Sunda–Andaman subduction zone. *Nat Hazards* 116, 401–423,
641 <https://doi.org/10.1007/s11069-022-05680-6>, 2023.
- 642 Boak EH, Turner IL.: Shoreline definition and detection: a review. *J Coast Res* 21:688–703,
643 <https://doi.org/10.2112/03-0071.1>, 2005.
- 644 Cho, Y. S., Lakshumanan, C., Choi, B. H., & Ha, T. M.: Observations of run-up and inundation levels
645 from the teletsunami in the Andaman and Nicobar Islands: A field report. *Journal of Coastal*
646 *Research*, 24(1), 216-223, <https://doi.org/10.2112/06-0662.1>, 2008.
- 647 Cooper JA, Jackson D, Nava F, McKenna J, Malvarez G.: Storm impacts on an embayed high energy
648 coastline, western Ireland. *Marine Geol* 210:261–280,
649 <https://doi.org/10.1016/j.margeo.2004.05.012>, 2004.
- 650 Crowell, M., Douglas, B. C., & Leatherman, S. P.: On forecasting future US shoreline positions: a test
651 of algorithms. *Journal of Coastal Research*, 1245-1255, <http://www.jstor.org/stable/4298734>,
652 1997.
- 653 Curray, J. R.: Tectonics and history of the Andaman Sea region. *Journal of Asian Earth Sciences*, 25(1),
654 187-232, <https://doi.org/10.1016/j.jseaes.2004.09.001>, 2005.
- 655 DANI, B., SRIVASTAVA, V., SINGH, A., & BHATLA, R.; Numerical modeling of tsunami wave to
656 assess the possible impacts along western coasts of India. *MAUSAM*, 74(4), 1131-1140, 2023.
- 657 Dao, M. H., & Tkalich, P., Tsunami propagation modeling—a sensitivity study. *Natural Hazards and*
658 *Earth System Sciences*, 7(6), 741-754, 2007.
- 659 Davis, R.A.: Human Impact on Coasts. In: Finkl, C.W., Makowski, C. (eds) *Encyclopedia of Coastal*
660 *Science*. *Encyclopedia of Earth Sciences Series*. Springer, Cham, [https://doi.org/10.1007/978-3-](https://doi.org/10.1007/978-3-319-93806-6_175)
661 [319-93806-6_175](https://doi.org/10.1007/978-3-319-93806-6_175), 2019.
- 662 Den Boer, E. L., & Oele, A. C.: Determination of shoreline change along the East-Java coast, using the
663 Digital Shoreline Analysis System. In *MATEC Web of Conferences* (Vol. 177, p. 01022). EDP
664 *Sciences*, <https://doi.org/10.1051/matecconf/201817701022>, 2018.
- 665 Devi, E. U., & Shenoi, S. S. C.: Tsunami and the effects on coastal morphology and ecosystems: a
666 report. *Proceedings of the Indian National Science Academy*, 78(3), 513-521, 2012.
- 667 Dolan, R., Fenster, M. S., & Holme, S. J.: Temporal analysis of shoreline recession and accretion.
668 *Journal of coastal research*, 723-744, <http://www.jstor.org/stable/4297888>, 1991.

669 Fletcher, C.H., Romine, B.M., Genz, A.S., Barbee, M.M., Dyer, M., Anderson, T.R., Lim, S.C.,
670 Vitousek, S., Bochicchio, C., & Richmond, B.M.: National assessment of shoreline change:
671 Historical shoreline change in the Hawaiian Islands. In (p. 55), 2011.

672 Ghadamode, V., Srivastava, K., Singh, R. K., & Pandey, A. K.: Spatial analysis techniques for tsunami
673 vulnerability and inundation mapping of Andaman region using remote sensing, GIS, AHP, and
674 Fuzzy logic methods. *Environmental Earth Sciences*, 81(17), 427,
675 <https://doi.org/10.1007/s12665-022-10548-w>, 2022.

676 Ghosh, T., Jana, P., Giritharan, S., Bardhan, S., Basir, S. R., & Roy, A. G.:Tsunami Survey in Andaman
677 Nicobar Group of Islands. *Sumatra–Andaman Earthquake and Tsunami*, 26, 2004.

678 Hamuna, B., Kalor, J. D., & Tablaseray, V. E.: The impact of tsunami on mangrove spatial change in
679 the eastern coast of Biak Island, Indonesia. *Journal of Ecological Engineering*, 20(3),
680 <http://dx.doi.org/10.12911/22998993/95094>, 2019.

681 Himmelstoss, E., Henderson, R. E., Kratzmann, M. G., & Farris, A. S.: Digital shoreline analysis system
682 (DSAS) version 5.1 user guide (No. 2021-1091). US Geological Survey,
683 <https://doi.org/10.3133/ofr20211091>, 2021.

684 Imamura, F.: Review of Tsunami Simulation with a Finite Difference Method. *Long Waves Runup*
685 *Models*, 1996.

686 Imamura, F., & Imteaz, M. A.: Long waves in two-layers: governing equations and numerical model.
687 *Science of Tsunami Hazards*, 13(1), 3-24,1995.

688 Jain, S. K., Murty, C. V. R., Rai, D. C., Malik, J. N., Sheth, A., & Jaiswal, A.: Effects of M9 Sumatra
689 earthquake and tsunami of December 26, 2004. *Current Science*, 88(3), 357-359,
690 <https://www.currentscience.ac.in/Volumes/88/03/0357.pdf>, 2005.

691 Jaman, T., Dharanirajan, K., & Rana, S.: Land use and Land cover Change detection and Its
692 Environmental Impact on South Andaman Island, India using Kappa coefficient Statistical
693 Analysis and Geospatial Techniques, 2022.

694 Jayakumar K, Malarvannan S.: Assessment of shoreline changes over the Northern Tamil Nadu Coast,
695 South India using WebGIS techniques. *J Coast Conserv.* 20(6):477–487,
696 <https://link.springer.com/article/10.1007/s11852-016-0461-9>, 2016.

697 Jevrejeva, S., Jackson, L., Riva, R., Grinsted, A., & Moore, J.: Sea level rise with warming above 2
698 degree. In *EGU General Assembly Conference Abstracts* (p. 3637), 2017.

699 Joesidawati, M. I.: Shoreline change in Tuban district, East Java using geospatial and digital shoreline
700 analysis system (DSAS) techniques. *International Journal of Oceans and Oceanography*, 10(2),
701 235-246, 2016.

702 Kumar ST, Mahendra RS, Nayak S, Radhakrishnan K, Sahu KC.: Coastal vulnerability assessment for
703 Odisha state, East coast of India. *J Coast Res* 26:523–534, <https://doi.org/10.2112/09-1186.1>,
704 2010.

705 Kumari P, Jnaneswari K, Rao D, Sridhar D.: Application of remote sensing and geographical
706 information system techniques on geomorphological mapping of coastal part of East Godavari
707 district. Andhra Pradesh, India. *Int J Eng Sci Tech* 4:4296–4300,
708 <https://link.springer.com/article/10.1007/s11069-016-2252>, 2012.

709 Leatherman, S. P.: Shoreline change mapping and management along the US East Coast. *Journal of*
710 *Coastal Research*, 5-13, 2003.

- 711 Mageswaran, T., Sachithanandam, V., Sridhar, R., Mahapatra, M., Purvaja, R., & Ramesh, R.: Impact
712 of sea level rise and shoreline changes in the tropical island ecosystem of Andaman and Nicobar
713 region, India. *Natural Hazards*, 109, 1717-1741,
714 <https://link.springer.com/article/10.1007/s11069-021-04895-3>, 2021.
- 715 Mansinha, L., and Smylie, D.E.: The displacements fields of inclined faults, *Bull. Seismol. Soci. Am.*,
716 61(5), 1433-1440, 1971.
- 717 Masaya, R., Suppasri, A., Yamashita, K., Imamura, F., Gouramanis, C., & Leelawat, N.: Investigating
718 beach erosion related with tsunami sediment transport at Phra Thong Island, Thailand, caused by
719 the 2004 Indian Ocean tsunami. *Natural Hazards and Earth System Sciences*, 20(10), 2823-2841,
720 2020.
- 721 Mishra, P., Usha, T., & Ramanamurthy, M. V.: Evaluation of tsunami vulnerability along the northeast
722 coast of India. *Continental Shelf Research*, 79, 16-22, 2014.
- 723 Misra, A., & Balaji, R.: A study on the shoreline changes and Land-use/land-cover along the South
724 Gujarat coastline. *Procedia Engineering*, 116, 381-389,
725 <https://doi.org/10.1016/j.proeng.2015.08.311>, 2015.
- 726 Moran CAA.: Spatio-temporal analysis of texas shoreline changes using GIS technique. *Mediterranean*
727 *Mar Sci* 2:5–13, <https://hdl.handle.net/1969.1/408>, 2003.
- 728 Mukhopadhyay, A., Mukherjee, S., Hazra, S., & Mitra, D.: Sea level rise and shoreline changes: a
729 geoinformatic appraisal of Chandipur coast, Orissa. *Int J Geol Earth Environ Sci*, 1(1), 9-17,
730 2011.
- 731 Murali M, Ankitha M, Amritha S, Vethamony P.: Coastal vulnerability of Puducherry coast, India,
732 using analytical hierarchical process. *Nat Hazards Earth Syst Sci* 13:3291–3311,
733 <https://doi.org/10.5194/nhess-13-3291-2013>, 2013, 2013.
- 734 Murty, C. V. R., Rai, D. C., Jain, S. K., Kaushik, H. B., Mondal, G., & Dash, S. R.; Performance of
735 structures in the Andaman and Nicobar Islands (India) during the December 2004 great Sumatra
736 earthquake and Indian Ocean tsunami. *Earthquake spectra*, 22(3_suppl), 321-354, 2006.
- 737 Nagabhatla, N., Roy, P. S., & Jagdale, R.: Evaluating the change (1968-2001) in landscape pattern and
738 analyzing disturbance in Baratang Forest Division (Andaman Islands), SOUTHEAST ASIA,
739 <https://hdl.handle.net/10568/40948>, 2006.
- 740 Nanda, A. R., & Haub, C.: The future population of India—a long-range demographic view. *Popul Res*
741 *Bureau*, 2007.
- 742 Natarajan, L., Sivagnanam, N., Usha, T., Chokkalingam, L., Sundar, S., Gowrappan, M., & Roy, P. D.:
743 Shoreline changes over last five decades and predictions for 2030 and 2040: a case study from
744 Cuddalore, southeast coast of India. *Earth Science Informatics*, 14(3), 1315-1325, 2021.
- 745 National Research Council: Tsunami warning and preparedness: an assessment of the US tsunami
746 program and the nation's preparedness efforts, Committee on the Review of the Tsunami Warning
747 and Forecast System and Overview of the Nation's Tsunami Preparedness, National Research
748 Council, 284 pp, 2011.
- 749 Nayak S.: Use of coastal data in coastal mapping. *Indian Carto CMMC* 147–156, 2002.
- 750 Raj, N., Rejin Nishkalank, R.A., Chrisben Sam, S.: Coastal Shoreline Changes in Chennai: Environment
751 Impacts and Control Strategies of Southeast Coast, Tamil Nadu. In: Hussain, C. (eds) *Handbook*

- 752 of Environmental Materials Management. Springer, Cham. [https://doi.org/10.1007/978-3-319-](https://doi.org/10.1007/978-3-319-58538-3_223-1)
753 [58538-3_223-1](https://doi.org/10.1007/978-3-319-58538-3_223-1), 2020.
- 754 Prabhbir Singh., and Kamlesh Khanduri.: Land use and Land cover change detection through Remote
755 Sensing & GIS Technology: Case study of Pathankot and Dhar Kalan Tehsils. Inter. Journal, of.
756 Geomatics and Geosciences 1(4), pp 839-846, 2011.
- 757 Prerna, R., Srinivasa Kumar, T., Mahendra, R. S., & Mohanty, P. C.: Assessment of Tsunami Hazard
758 Vulnerability along the coastal environs of Andaman Islands. Natural Hazards, 75, 701-726,
759 <https://link.springer.com/article/10.1007/s11069-014-1336-8>, 2015.
- 760 Ramalanjaona, G.: Impact of 2004 tsunami in the islands of Indian Ocean: Lessons learned. Emergency
761 Medicine International, <https://doi.org/10.1155/2011/920813>, 2011.
- 762 Rani, V. S., Srivastava, K., & Dimri, V. P.: Tsunami propagation and inundation due to tsunamigenic
763 earthquakes in the Sumatra-Andaman subduction zone: Impact at Visakhapatnam. Marine
764 Geodesy, 34(1), 48-58. <https://doi.org/10.1080/01490419.2011.547802>, 2011.
- 765 Reguero, B. G., Beck, M. W., Agostini, V. N., Kramer, P., & Hancock, B., Coral reefs for coastal
766 protection: A new methodological approach and engineering case study in Grenada. Journal of
767 Environmental Management, 210, 146-161, <https://doi.org/10.1016/j.jenvman.2018.01.024>,
768 2018.
- 769 Rowland, E. D., Lolade, A. A., Nicholas, D. O., Opukumo, A. W., & Omonefe, F.: The Environmental
770 Impact of Shoreline Changes and Land Use/Land Cover Change Detection in the Niger Delta
771 Region using Geospatial Technology. Journal of Asian Scientific Research, 12(4), 237-248,
772 2022.
- 773 Sachithanandam, V., Mageswaran, T., Ragavan, P., Mahapatra, M., Sridhar, R., Ramesh, R., & Mohan,
774 P. M.: Mangrove regeneration in tsunami-affected area of north and south Andaman using insitu
775 and remote sensing techniques, 2014.
- 776 Sarkar, D., Mukhopadhyay, A., & Hazra, S.: Nature of tsunami and paleo tsunami deposits of South
777 Andaman. Int J Basic Appl Sci Res, 2(3), 2275-2285, 2012.
- 778 Sathiparan, N.: An assessment of building vulnerability to a tsunami in the Galle coastal area, Sri Lanka.
779 Journal of Building Engineering, 27, 100952, <https://doi.org/10.1016/j.jobbe.2019.100952>,
780 2020.
- 781 Scheffers A, Scheffers S, Kelletat D.: Paleotsunami relics on the southern and central Antillean island
782 arc. J Coast Res 21:263–273, <https://doi.org/10.2112/03-0144.1>, 2005.
- 783 Shaw, G., & Williams, A.: Impact of the Tsunami on the Tourism Industry and Ecosystem of the
784 Andaman and Nicobar Islands, India,2006.
- 785 Sheth, A., Sanyal, S., Jaiswal, A., & Gandhi, P.: Effects of the December 2004 Indian Ocean tsunami
786 on the Indian mainland. Earthquake spectra, 22(3_suppl), 435-473,
787 <https://doi.org/10.1193/1.2208562>, 2006.
- 788 Singh, A. P., Murty, T. S., Rastogi, B. K., & Yadav, R. B. S.: Earthquake generated tsunami in the
789 Indian Ocean and probable vulnerability assessment for the east coast of India. Marine Geodesy,
790 35(1), 49-65, <https://doi.org/10.1080/01490419.2011.637849>,2012.
- 791 Siva M.: Behera MR. Effect of continental slope on N-wave type tsunami run-up. The International
792 Journal of Ocean and Climate Systems, <https://doi.org/10.1177/1759313116656865>, 2016.

793 South Andaman District – Population.: [https://www.census2011.co.in/census/district/53-south-](https://www.census2011.co.in/census/district/53-south-andaman.html)
794 [andaman.html](https://www.census2011.co.in/census/district/53-south-andaman.html), 2011-2023.

795 Srivastava, K., Begum, F., & Jakkula, M.: Tsunami Modelling and Run-ups along Indian Coasts.
796 Journal of the Geological Society of India, 97, 1307-1312, [https://doi.org/10.1007/s12594-021-](https://doi.org/10.1007/s12594-021-1861-5)
797 [1861-5](https://doi.org/10.1007/s12594-021-1861-5), 2021.

798 Sudha Rani NNV, Satyanarayana ANV, Bhaskaran PK.: Coastal vulnerability assessment studies over
799 India: a review. Nat Hazards, [https://link.springer.com/article/10.1007/s11069-015-1597,](https://link.springer.com/article/10.1007/s11069-015-1597-)
800 2015.

801 Sugawara, D.: Numerical modeling of tsunami: Advances and future challenges after the 2011 Tohoku
802 earthquake and tsunami. Earth-Science Reviews, 214, 103498, 2021.

803 Thakur, S., Dharanirajan, K., Ghosh, P. B., Das, P., & De, T. K.: Influence of anthropogenic activities
804 on the land use pattern of South Andaman Islands. Research Journal of Marine Sciences, 5(1), 1-
805 10, 2017.

806 The Economic Times: [https://economictimes.indiatimes.com/tsunami-hits-india-inc-with-rs-3000-cr-](https://economictimes.indiatimes.com/tsunami-hits-india-inc-with-rs-3000-cr-loss/articleshow/974281.cms?from=mdr)
807 [loss/articleshow/974281.cms?from=mdr](https://economictimes.indiatimes.com/tsunami-hits-india-inc-with-rs-3000-cr-loss/articleshow/974281.cms?from=mdr)

808 Thieler ER, Himmelstoss EA, Zichichi JL, Ergul A.: Digital shoreline analysis system (DSAS) version
809 4.0-an ArcGIS extension for calculating shoreline change. US Geological Survey open-file report
810 2008–1278. US Geological Survey, Woods Hole, <https://doi.org/10.3133/ofr20081278>, 2009.

811 Thiéblemont, R., Le Cozannet, G., Rohmer, J., Toimil, A., Álvarez-Cuesta, M., and Losada, I. J.: Deep
812 uncertainties in shoreline change projections: an extra-probabilistic approach applied to sandy
813 beaches, Nat. Hazards Earth Syst. Sci., 21, 2257–2276, [https://doi.org/10.5194/nhess-21-2257-](https://doi.org/10.5194/nhess-21-2257-2021)
814 [2021](https://doi.org/10.5194/nhess-21-2257-2021), 2021

815 Tonisso H, Suursarr U, Kont A.: Maps, aerial photographs, orthophotos, and GPS data as a source of
816 information to determine shoreline changes, coastal geomorphic processes and their relation to
817 hydrodynamic conditions on Osmussa island, The Baltic sea. IGRSS 12:987–1159,
818 <https://doi.org/10.1109/IGARSS.2012.6350382>, 2012.

819 Velmurugan, A., Swarnam, T. P., & Ravisankar, N.: Assessment of tsunami impact in South Andaman
820 using remote sensing and GIS. J. Indian Soc. Remote Sensing, 34(2), 193-202, 2006.

821 Vu, M. T., Lacroix, Y., & Vu, Q. H.; Assessment of the Shoreline Evolution at the Eastern Giens
822 Tombolo of France. In Proceedings of the International Conference on Innovations for
823 Sustainable and Responsible Mining: ISRM 2020-Volume 2 (pp. 349-372). Springer
824 International Publishing, 2021.

825 Wood, N., Jones, J. M., Yamazaki, Y., Cheung, K. F., Brown, J., Jones, J. L., & Abdollahian, N.:
826 Population vulnerability to tsunami hazards informed by previous and projected disasters: a case
827 study of American Samoa. Natural Hazards, 95, 505-528,
828 <https://link.springer.com/article/10.1007/s11069-018-3493-7>, 2019.

829 United Nations Office for Disaster Risk Reduction (UNDRR):
830 [https://www.preventionweb.net/understanding-disaster-risk/component-risk/vulnerability,](https://www.preventionweb.net/understanding-disaster-risk/component-risk/vulnerability)
831 2017.

832 Yunus, A. P., & Narayana, A. C.: Short-term morphological and shoreline changes at Trinkat Island,
833 Andaman and Nicobar, India, after the 2004 tsunami. *Marine Geodesy*, 38(1), 26-39,
834 <https://doi.org/10.1080/01490419.2014.908795>, 2015.

- 835 Yunus, A. P., Dou, J., Avtar, R., & Narayana, A.: Shoreline and coastal morphological changes induced
836 by the 2004 Indian Ocean tsunami in the Katchal Island, Andaman and Nicobar—a study using
837 archived satellite images. In *Tsunamis and earthquakes in coastal environments* (pp. 65-77).
838 Springer, Cham, https://link.springer.com/chapter/10.1007/978-3-319-28528-3_5, 2016.
- 839 Yuvaraj, E., Saravanan, E., & Dharanirajan, K.: Assessment of land use and land cover changes in south
840 Andaman Island using remote sensing and GIS. *Int J Geomat Geosci*, 5, 171-181, 2014.
- 841 Yi, L., Chen, J., Jin, Z., Quan, Y., Han, P., Guan, S., & Jiang, X.: Impacts of human activities on the
842 coastal ecological environment during the rapid urbanization process in Shenzhen, China. *Ocean
843 & Coastal Management*, 154, 121-132, <https://doi.org/10.1016/j.ocecoaman.2018.01.005>,
844 2018.
- 845 Zhang, Y., Yin, K., Tang, Y., & Xiao, L.: Tsunami Squares: Leapfrog scheme implementation and
846 benchmark study on wave–shore interaction of solitary waves. *Scientific Reports*, 14(1), 13053,
847 2024.
- 848